

The Trajectory Alignment Coefficient in Two Acts: From Reward Tuning to Reward Learning

Calarina Muslimani^{1,2*}, Yunshu Du¹, Kenta Kawamoto¹, Kaushik Subramanian¹, Peter Stone^{1,3}, Peter Wurman¹

¹ Sony AI

² University of Alberta

³ The University of Texas at Austin

Abstract

The success of reinforcement learning (RL) is fundamentally tied to having a reward function that accurately reflects the task objective. Yet, designing reward functions is notoriously time-consuming and prone to misspecification. To address this issue, our first goal is to understand how to support RL practitioners in specifying appropriate weights for a reward function. We leverage the Trajectory Alignment Coefficient (TAC), a metric that evaluates how closely a reward function’s induced preferences match those of a domain expert. To evaluate whether TAC provides effective support in practice, we conducted a human-subject study in which RL practitioners tuned reward weights for Lunar Lander. We found that providing TAC during reward tuning led participants to produce more performant reward functions and report lower cognitive workload relative to standard tuning without TAC. However, the study also underscored that manual reward design, even with TAC, remains labor-intensive. This limitation motivated our second goal: to learn a reward model that maximizes TAC directly. Specifically, we propose Soft-TAC, a differentiable approximation of TAC that can be used as a loss function to train reward models from human preference data. Validated in the racing simulator Gran Turismo 7, reward models trained using Soft-TAC successfully captured preference-specific objectives, resulting in policies with qualitatively more distinct behaviors than models trained with standard Cross-Entropy loss. This work demonstrates that TAC can serve as both a practical tool for guiding reward tuning and a reward learning objective in complex domains.

1 Introduction

The reward function lies at the foundation of reinforcement learning (RL), as agents aim to maximize the expected cumulative reward [Sutton and Barto, 2018]. In practice, however, solving a task with RL assumes access to a reward

*Work done while interning at Sony AI. Corresponding author: musliman@ualberta.ca.

function that accurately captures the task objective. Without such a reward function, learning can fail entirely, leading agents to pursue undesired or unsafe behaviors [Amodei *et al.*, 2016; Skalse *et al.*, 2022]. This issue can be particularly pronounced in real-world domains such as autonomous driving [Knox *et al.*, 2023], where reward functions must capture subjective, preference-specific objectives (e.g., driving style or adherence to etiquette). Most practitioners rely on a trial-and-error approach, iteratively adjusting reward functions based on the behavior of RL agents trained with those rewards. This process is costly, time-consuming, and often results in reward misspecification [Booth *et al.*, 2023]. Despite its importance, best practices for reward design have received relatively little attention, particularly regarding tools that help practitioners iteratively refine reward specifications.

The first goal of this work is to evaluate the utility of the Trajectory Alignment Coefficient (TAC) [Muslimani *et al.*, 2025], a reward alignment metric, for supporting RL practitioners during manual reward design, specifically when tuning a reward function from scratch. While other reward evaluation metrics exist, we focus on TAC because alternative approaches either require access to a ground-truth reward [Gleave *et al.*, 2021; Wulfe *et al.*, 2022; Skalse *et al.*, 2024], which we cannot assume, or fail to provide a continuous alignment signal [Brown *et al.*, 2021; Knox and MacGlashan, 2024], which is needed for iterative reward refinement.

We investigate whether TAC can guide RL practitioners in specifying reward functions. To do so, we conducted an ethics-approved human-subject study in Lunar Lander, a continuous state and action domain with eight tunable reward weights [Brockman *et al.*, 2016], making reward design difficult. Practitioners were provided with a set of reward features and tasked with determining appropriate weights under one of two conditions: with TAC feedback or without. Participants in the TAC condition received TAC scores for each candidate reward function as they iteratively adjusted the weights. This guidance led to statistically significant improvements: the final reward functions produced policies with higher task success rates, and perceived cognitive workload decreased by $\sim 30\%$ relative to reward tuning without TAC.

While these results demonstrate that TAC can support effective reward design, the process still required substantial effort; with participants iterating over their designs ~ 40 times. This observation motivates the second goal of our work: to

automatically learn a reward model that maximizes TAC. We introduce a differentiable approximation of TAC, *Soft-TAC*, which can be used as a loss function to train reward models directly from human preferences.

We evaluate Soft-TAC across two domains: Lunar Lander, to confirm its ability to learn effective reward functions where human practitioners struggled; and the high-fidelity driving simulator Gran Turismo 7 (GT7) [Wurman *et al.*, 2022], to assess its effectiveness in producing qualitatively distinct behaviors given diverse human preferences. Our results show that reward models trained with Soft-TAC successfully captured human preferences in both domains. In Lunar Lander, these reward models enabled RL agents to achieve higher task success rates than both the standard Cross-Entropy loss [Christiano *et al.*, 2017] and manually tuned rewards. In GT7, Soft-TAC trained reward models better captured preferences reflecting different driving objectives, leading to qualitatively more distinct racing behaviors than models trained using Cross-Entropy. Together, our work highlights that TAC can serve as both a tool to support reward design and as an objective for learning human-aligned reward models.

2 Related Work

Preference-based RL (PbRL) learns reward functions from human preferences between trajectories. The standard formulation, introduced by Christiano *et al.* [2017], assumes that humans tend to prefer trajectories with higher total reward. This assumption supports a probabilistic preference model (e.g., Bradley and Terry [1952]), enabling reward learning via the Cross-Entropy loss on the negative log-likelihood of the observed preferences. A majority of PbRL methods closely follow this framework, adding only techniques to reduce the number of human queries or improve policy learning [Ibarz *et al.*, 2018; Lee *et al.*, 2021; Liang *et al.*, 2022; Park *et al.*, 2022; Hwang *et al.*, 2023; Shin *et al.*, 2023; Hejna III and Sadigh, 2023; Cheng *et al.*, 2024; Hu *et al.*, 2024; Verma and Metcalf, 2024; Choi *et al.*, 2024; Muslimani and Taylor, 2025; Kang and Oh, 2025; Pace *et al.*, 2025]. Some approaches vary from this setup by modifying the preference model or loss function. However, these methods often come with limitations, such as: (1) requiring online, policy-coupled training [Biyik and Sadigh, 2018; Liu *et al.*, 2022; Xie *et al.*, 2025]; (2) relying on fixed sets of policies for value estimation [Knox *et al.*, 2024]; (3) removing reward learning altogether [Hejna *et al.*, 2024]; or (4) treating preference annotations as independent “win” or “loss” labels, which ignore that a trajectory’s label depends on what it is being compared to and can result in conflicting labels [Sun *et al.*, 2025].

3 Background

This section first provides background on RL, then describes the reward alignment metric, the Trajectory Alignment Coefficient. It concludes with a discussion of reward learning.

3.1 Reinforcement Learning

We consider a Markov decision process defined by the tuple $(\mathcal{S}, \mathcal{A}, r, p, \mu, \gamma)$. Here, \mathcal{S} and \mathcal{A} denote the state and action

spaces, $r : \mathcal{S} \times \mathcal{A} \times \mathcal{S} \rightarrow \mathbb{R}$ specifies the reward per transition and $p : \mathcal{S} \times \mathcal{A} \times \mathcal{S} \rightarrow [0, 1]$ defines the transition dynamics. The initial-state distribution is given by μ , and the discount factor $\gamma \in [0, 1)$ controls the weighting of future rewards. In this framework, an agent interacts with the environment in discrete time steps. At time t , it observes a state s_t , selects an action a_t , transitions to a new state s_{t+1} , and receives a reward r_{t+1} . A trajectory τ consists of a sequence of (s_t, a_t, s_{t+1}) triplets, ending in a terminal state or continuing indefinitely. A trajectory’s discounted return (with respect to reward function r) is defined as the discounted sum of future rewards, $G_r(\tau) = \sum_{t=0}^T \gamma^t r_{t+1}$ where $T = |\tau| - 1$ for episodic tasks or $T \rightarrow \infty$ in continuing tasks. The objective in RL is to learn a policy $\pi : \mathcal{S} \rightarrow \Delta(\mathcal{A})$ that maximizes the expected discounted return.

3.2 Learning Reward Functions from Preferences

A common approach to reward learning is preference-based RL, in which a reward model \hat{r}_θ is learned from a dataset of human preferences [Christiano *et al.*, 2017]. The reward model can be a weighted linear combination of features (learning the feature weights) or a black-box neural network (learning the network parameters directly).

Definition 1. Formally, the human preference dataset is

$$\mathcal{D}_h = \{(\tau^i, \tau^j, y)\}_{i=1}^N,$$

where each (τ^i, τ^j) is a pair of trajectories and y is the observed label indicating which trajectory was preferred.

Reward functions can be learned from \mathcal{D}_h via supervised learning. For instance, the widely used Cross-Entropy loss:

$$\begin{aligned} \mathcal{L}^{CE}(\theta, \mathcal{D}_h) = -\mathbb{E}_{(\tau^i, \tau^j, y) \sim \mathcal{D}_h} & \left[(1 - y) \log P_\theta(\tau^j > \tau^i) \right. \\ & \left. + y \log P_\theta(\tau^i > \tau^j) \right], \end{aligned} \quad (1)$$

where the labels are interpreted as $y \in \{0, 0.5, 1\}$: 1 indicates $\tau^i \succ \tau^j$, 0 indicates $\tau^j \succ \tau^i$, and 0.5 indicates a tie. The predicted probabilities P_θ are computed using the Bradley–Terry (BT) model [Bradley and Terry, 1952], which converts cumulative predicted rewards into preference probabilities. This model implicitly assumes Boltzmann rationality: the probability of a human preferring τ^i over τ^j depends exponentially on the predicted returns summed over the trajectory:

$$P_\theta(\tau^i > \tau^j) = \frac{\exp \left(\sum_t \hat{r}_\theta(s_t^i, a_t^i) \right)}{\sum_{\tau' \in \{\tau^i, \tau^j\}} \exp \left(\sum_t \hat{r}_\theta(s_t^{\tau'}, a_t^{\tau'}) \right)}. \quad (2)$$

3.3 Trajectory Alignment Coefficient (TAC)

TAC is a reward–alignment metric that assesses how well a candidate reward function and discount factor pair (r, γ) respects a human stakeholder’s preferences. It is based on Kendall’s Tau–b [Kendall, 1945] which measures agreement between ranked data. TAC compares finite datasets of binary preferences: the human-provided preferences \mathcal{D}_h , assumed to be transitive, and the preference dataset induced by (r, γ) ,

denoted $\mathcal{D}_{r,\gamma}$. From the human data, we extract the set of un-ordered trajectory pairs that were compared. For each such pair, we then construct the corresponding preference under the candidate reward, by comparing their expected returns. Specifically, trajectory τ_A is preferred over τ_B if and only if $G_r(\tau_A) > G_r(\tau_B)$. Once we have both \mathcal{D}_h and $\mathcal{D}_{r,\gamma}$, TAC measures their agreement using Kendall's Tau-b:

$$\sigma_{TAC}(\mathcal{D}_h, \mathcal{D}_{r,\gamma}) \doteq \frac{P - Q}{\sqrt{(P + Q + X_0)(P + Q + Y_0)}} \quad (3)$$

where

P : Number of concordant pairs between $\mathcal{D}_{r,\gamma}$ and \mathcal{D}_h ,

Q : Number of discordant pairs between $\mathcal{D}_{r,\gamma}$ and \mathcal{D}_h ,

X_0 : Number of pairs tied only in $\mathcal{D}_{r,\gamma}$,

Y_0 : Number of pairs tied only in \mathcal{D}_h .

Equation 3 outputs a score between -1 and 1 , where 1 indicates that the pair (r, γ) induces the same preference relations as the human over all trajectory pairs and -1 indicates complete disagreement with the human preferences.

4 Can TAC help with manual reward tuning?

Our first goal is to understand whether RL practitioners can use TAC to effectively determine reward weights *from scratch*. Prior work has shown that even in a tabular environment, practitioners were unable to effectively tune as few as four reward weights [Booth *et al.*, 2023], highlighting that reward weight tuning remains a significant challenge. We study TAC as a reward design tool as it has shown promise in assisting RL practitioners with reward selection [Muslimani *et al.*, 2025]. However, existing empirical validation is limited. The original study restricted participants to selecting between pre-specified reward functions, which is not representative of a realistic reward design setting. Furthermore, evaluations were conducted solely in a tabular domain, leaving the effectiveness of TAC in high-dimensional environments unexplored.

To investigate this gap, we conducted an ethics-approved study with 11 self-identified RL practitioners. Each participant was asked to *determine the weights of a linear reward function* for a given set of features. We assume the features are sufficient to represent the task objective, therefore the challenge lies solely in determining how the features should be weighted. To support them in this task, we provided one of two types of assistance, with participants randomly assigned to a condition. We chose a between-subjects design to prevent carryover effects, ensuring that each participant's experience was unaffected by exposure to the other condition.

4.1 User Study Design

This section describes the design of our human-subject study, including the test domain, study protocol, experimental conditions, research questions, and evaluation procedures.

Test Domain

We consider the continuous-action version of Lunar Lander, where the goal is for a lander to land between two flags on the moon. This environment was chosen due to the complexity of its reward function. First, it is a linear combination

of *eight distinct reward components*, substantially more than many environments, including all MuJoCo tasks from OpenAI Gym, which have between $2 - 4$ components [Brockman *et al.*, 2016]. Second, in Lunar Lander's default reward function, the magnitude of these components vary considerably, making uniform weighting ineffective and increasing the difficulty of selecting appropriate reward weights. These properties make Lunar Lander a suitable choice for studying the challenge of tuning reward weights. We describe the environment in more detail in the Appendix A.1.

Study Protocol

The study consisted of two primary components. First, participants read a description of Lunar Lander and were informed that they would be collaborating with a domain expert to tune a reward function for RL training. The domain expert (one of the authors) reviewed 148 pairs of video clips and manually selected the preferred trajectory for each pair, ensuring the labels reflected human judgment rather than using synthetic preferences. The video clips were generated from rollouts of RL agents trained under different reward functions, selected to exhibit qualitatively distinct behaviors, following the heuristic proposed by Muslimani *et al.* [2025]. We then randomly selected 15 pairs to present to participants, choosing a subset to avoid overwhelming them with too many videos. Participants were instructed to review the clips to understand the domain expert's preferences regarding landing behavior.

Second, participants were presented with descriptions of the eight reward components, including pseudocode for how each was calculated, and asked to assign a weight to each component. Their objective was to tune the weights so that the resulting reward function aligned with the domain expert's preferences, which emphasized successful landings on the landing pad. The study was iterative: participants could select initial weights, review the trajectory videos, and receive feedback according to their assigned condition, adjusting the weights repeatedly until satisfied. This procedure allowed participants to explore how different weight choices affected the evaluation of agent behaviors. Figures 3–8 in Appendix A.2 show the user interface.

Experimental Conditions and Research Questions

Participants were assigned to one of two conditions. In the *Control* condition, they received the computed returns for each pair of trajectories (from the corresponding video clips) under their chosen reward weights. In the *Alignment* condition, they received the same information, plus the TAC score, computed from the domain expert's preferences and those induced by the participant's selected reward function. We investigate whether providing TAC scores influences how RL practitioners tune reward weights by comparing outcomes and experiences between participants with and without TAC feedback. Specifically, we focus on two key questions:

- **RQ1:** Does TAC help RL practitioners select reward weights that allow an RL agent to complete the task?
- **RQ2:** Does TAC reduce the perceived cognitive workload incurred during reward tuning?

Evaluation

To evaluate RQ1, we trained an RL agent using each participant’s final submitted reward function. Specifically, we trained a SAC agent [Haarnoja *et al.*, 2018] for five seeds. For a reliable estimate of final performance, five policies near the end of training were evaluated (without exploration) for five episodes each. For each participant, we measured *landing-pad success rate*, defined as the number of episodes in which the lander successfully landed with at least one leg between the two flags (marking the landing zone). We averaged these outcomes across the 125 evaluation episodes (five seeds \times five policies per seed \times five episodes per policy) to obtain a single performance score per participant. Finally, we compared the participants’ scores between the Alignment and Control conditions to assess whether providing TAC during reward tuning led participants to design reward functions that improved the resulting RL agent’s performance. Next, to evaluate RQ2, we administered the NASA Task Load Index (NASA-TLX) [Hart and Staveland, 1988], which measures cognitive workload on a 1–7 scale. Participants completed this survey after finishing the reward-tuning task. Across all analyses, we performed Welsh *t*-tests when normality assumptions held and Mann-Whitney *U*-tests otherwise.

4.2 Results

Figure 1a shows the average landing pad success rate for agents trained with participant-tuned reward functions in the Alignment and Control conditions. Participants in the Alignment condition were able to tune the reward weights to achieve substantially higher success rates (Alignment: mean $\mu = 0.63$, standard error SE = 0.18; Control: $\mu = 0.20$, SE = 0.20). The improvement was statistically significant (Mann-Whitney $U = 24.5$, $p = 0.042$), suggesting that TAC enabled users to produce more effective reward functions.

Furthermore, we examined participants’ user experience during reward tuning. Figure 1b shows the NASA-TLX results along with the overall workload score, computed as the average of its subscales. Participants in the Alignment condition found reward tuning with TAC less mentally demanding, less frustrating, and overall more successful. Furthermore, the overall workload was significantly lower in the Alignment condition (Alignment: $\mu = 2.81$, SE = 0.24; Control: $\mu = 4.07$, SE = 0.41). The two conditions differed significantly ($t = -2.64$, $p = 0.018$), indicating that tuning reward functions with TAC made the process noticeably easier.

5 Can TAC be used to learn reward weights?

Our user study suggests that TAC can help RL practitioners manually tune reward weights. However, reward tuning remained a labor-intensive process: participants without TAC feedback adjusted weights an average of 49.6 times, while those with TAC did so 44 times. This motivates *learning* reward functions to maximize TAC instead of manual tuning. In doing so, we train reward models using *real human preference data*. This is in contrast to typical PbRL, which assumes access to the environment’s reward function to create synthetic preferences (see Appendix B.1 for further discussion).

5.1 Differentiable TAC

To enable gradient-based optimization, we introduce *Soft-TAC*, an approximation of TAC, denoted by $\tilde{\sigma}_{\text{TAC}}(\mathcal{D}_h, G_r)$:

$$\mathbb{E}_{(\tau^i, \tau^j, y) \sim \mathcal{D}_h} \left[y \cdot \tanh \left(\alpha \Delta G_r(\tau^i, \tau^j) \right) \right] \quad (4)$$

where $y \in \{-1, 0, 1\}$ is the preference label ($y = 1$ for $\tau^i \succ \tau^j$, -1 for $\tau^j \succ \tau^i$, 0 for ties), $\Delta G_r(\tau^i, \tau^j)$ is the difference in returns between trajectories τ^i and τ^j , and α controls the sensitivity of the loss to differences in returns.

Proposition 1. *Given no ties, $\tilde{\sigma}_{\text{TAC}, \alpha}(\mathcal{D}_h, G_r)$ is a differentiable approximation of the Trajectory Alignment Coefficient:*

$$\sigma_{\text{TAC}} = \lim_{\alpha \rightarrow \infty} \tilde{\sigma}_{\text{TAC}, \alpha}(\mathcal{D}_h, G_r).$$

See Proof in Appendix B.2. A similar tanh-based relaxation of Kendall’s Tau was introduced by Zheng *et al.* [2023], motivating our choice. The tanh term provides a smooth approximation to the sign function, making the objective differentiable with respect to the reward model weights θ . We then use Soft-TAC as the objective for reward learning by minimizing its negative, encouraging the model to assign higher returns to trajectories preferred by humans. Formally,

$$\mathcal{L}_{\text{Soft-TAC}}(\theta; \mathcal{D}_h) = 1 - \tilde{\sigma}_{\text{TAC}, \alpha}(\mathcal{D}_h, G_{r_\theta}). \quad (5)$$

Equation 5 provides a generic loss formulation suitable for both online and offline reward learning methodologies. Next, we discuss two theoretical properties of Soft-TAC.

Definition 2. *Let $\mathcal{R}_{\text{human}}$ be the set of human-aligned reward functions r such that for every comparison $(\tau^i, \tau^j, y) \in \mathcal{D}_h$, the condition $y \cdot (G_r(\tau^i) - G_r(\tau^j)) > 0$ is satisfied.*

Assumption 1. \mathcal{D}_h is noise-free and transitive.

Assumption 2. *The hypothesis class $\{r_\theta\}_{\theta \in \Theta}$ is sufficiently expressive such that there exists at least one parameter vector $\theta^* \in \Theta$ such that the reward function $r_{\theta^*} \in \mathcal{R}_{\text{human}}$.*

Theorem 1. *Under Assumptions 1 and 2 and as $\alpha \rightarrow \infty$, a reward function r_{θ^*} is a global minimizer of the Soft-TAC loss if and only if it belongs to the set $\mathcal{R}_{\text{human}}$.*

Theorem 1 establishes that Soft-TAC is complete: the objective does not omit any valid human-aligned reward functions, and minimal: it cannot be further simplified without allowing misaligned reward functions to appear optimal. While this result assumes noise-free preferences, a reward learning objective should be able to handle inaccuracies in human feedback. The following theorem demonstrates that Soft-TAC is resilient to errors in human labeling.

Theorem 2. *Assume non-uniform label noise where the label noise rate η_x is a function of the input x and $\eta_x < \frac{n-1}{n}$ for all $x \in \mathcal{X}$, where n is the number of label classes. Under this condition and as $\alpha \rightarrow \infty$, $\mathcal{L}_{\text{Soft-TAC}}$ is noise-tolerant: the minimizer of the expected risk under noisy labels is identical to that under clean labels ($\theta_{\text{noisy}}^* = \theta_{\text{clean}}^*$).*

See proofs for both Theorems 1–2 in Appendix B.3–B.4. Note that the noise tolerance guarantee does not hold for Cross-Entropy. Furthermore, the geometry of the tanh function in Soft-TAC also provides practical robustness against

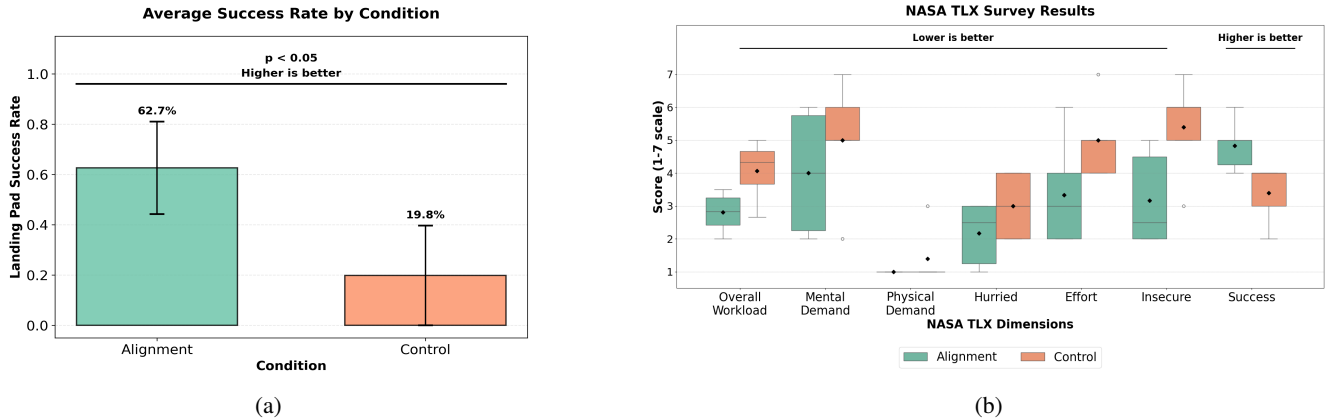


Figure 1: Lunar Lander user study results under different conditions: (a) Average success rate (\pm SE) of RL policies trained with the participant-tuned reward weights, and (b) participants' perceived workload measured using the NASA-TLX survey (box-and-whisker plot).

outliers. When the reward model predicts a large difference in the wrong direction (i.e., $G_{r_\theta}(\tau^i) - G_{r_\theta}(\tau^j) \gg 0$ but τ^j is preferred over τ^i), the tanh function saturates, and its gradient approaches zero. While this behavior might seem undesirable, it prevents wasted optimization on highly noisy preferences or those impossible for the model to fit. Such preferences can result from human error or hidden context not captured by the reward features (e.g., the human's mental model). In contrast, Cross-Entropy loss never decays for incorrect predictions, which can lead to conflicting gradient updates that cause the optimization to oscillate and converge to suboptimal solutions. We observed this phenomenon with the Cross-Entropy loss in our experiments in Section 5.3 and in a toy example in Appendix B.5.

5.2 Experiments and Results – Lunar Lander

Our user study established that manually tuning the multiple reward weights in Lunar Lander can be challenging. Therefore, it provides a natural benchmark to test if Soft-TAC can succeed where manual tuning struggles.

- **RQ3:** In Lunar Lander, can we learn effective reward models from human preferences using Soft-TAC?

Baselines

Our objective is to isolate the impact of the *loss function* on PbRL. Therefore, we employ the standard Cross-Entropy loss (Equation 1) combined with the BT model (Equation 2) as our primary baseline. This configuration is widely adopted by most PbRL algorithms, as discussed in Section 2. By stripping away additional confounding mechanisms from other algorithms, we ensure a direct comparison of the loss functions themselves. Additionally, we evaluate the environment's default reward function to assess whether the learned reward function can match or exceed its performance.

Preference Data Collection

To learn a reward function for successful landing, we used the full human-labeled preference dataset from the user study described in Section 4.1, which contains 148 preferences.

Training and Evaluation

In the PbRL setting, we first train a reward model from human preferences and then use this learned model in place of the environment's reward when training an RL agent. In our experiments, we use a linear reward model over the environment's eight predefined state features, matching our user study setup.

In all experiments, we optimize the reward weights using Adam [Kingma and Ba, 2015]. To select suitable hyperparameters, we performed a grid search over learning rates and batch sizes, and applied early stopping to prevent overfitting. We performed this reward learning procedure with five random seeds, producing distinct reward models. For each model, we then trained a corresponding RL agent using SAC. This procedure ensures that our results reflect the variability of the entire pipeline, from reward learning to policy optimization. See Appendix D for training details.

To evaluate performance, we used the same protocol as in the user study. For each trained RL agent, we evaluated five policies near the end of training over five episodes each, resulting in a total of 25 evaluation episodes (five policies \times five episodes). We then measured the average landing-pad success rate across the five seeds. To test for statistical differences, we performed Mann-Whitney U -tests, as the normality assumptions did not hold.

Results

We found that with Soft-TAC, learned reward models resulted in higher landing-pad success rates compared to Cross-Entropy (see Table 1), although the difference was not statistically significant (Mann-Whitney: $U = 11.5$, $p = 0.63$). Beyond success rates, the two methods differed in the kinds of failures they produced. Under Cross-Entropy, 100% of unsuccessful episodes ended in crashes, meaning the agent never landed at all. In contrast, only $\sim 37\%$ of Soft-TAC's failed episodes resulted in crashes, with the remaining failures still successfully landing, just not on the designated pad. Finally, Soft-TAC achieved a $\sim 10\%$ higher success rate than the reward weights manually tuned by RL practitioners with TAC in the user study.

Table 1: Shows the mean landing-pad success rates (\pm SE) in Lunar Lander after RL training with each reward function (higher is better).

Method	Landing-pad Success Rate
SOFT-TAC	0.72 ± 0.16
CROSS-ENTROPY	0.6 ± 0.24
DEFAULT REWARD	1.00 ± 0.0

5.3 Experiments and Results – Gran Turismo 7

Next, we consider GT7, a high-fidelity racing simulator characterized by diverse car models and realistic car-track dynamics. Developed by Polyphony Digital, Inc, this domain represents a significant increase in complexity over Lunar Lander. In particular, we consider two types of racing tasks: (1) *time-trial*, where the agent races alone with the objective of completing the track as quickly as possible, and (2) *versus*, where the agent races against 19 opponents.

We selected this domain because driving preferences are inherently subjective, making it an ideal testbed for evaluating whether our method can capture distinct driving styles from preference data. We formalize our investigation in this domain through the following research questions:

- **RQ4:** Can we learn preference-specific reward models with Soft-TAC that produce distinct driving behaviors?
 - **RQ4-a:** Can Soft-TAC learned rewards induce a *fast* driving style in the time-trial task?
 - **RQ4-b:** Can they also induce *aggressive* and *timid* driving behaviors in the versus setting?

Preference Data Collection

For both time-trial (RQ4-a) and versus tasks (RQ4-b), we collect preference trajectory data from Circuit de la Sarthe (Sarthe): a 13.6 km high-speed circuit that requires slipstreaming on long straights and managing car downforce, posing a challenge for training a driving agent on the track. We generated trajectories using a subset of 19 cars drawn from the total pool of 552 cars available in GT7. They were chosen to span a range of Performance Points (PP), an in-game metric measuring car competitiveness, with higher PP indicating a more powerful and faster car. This selection ensures that the trajectories capture a diverse set of driving behaviors (see Appendix C.1).

For **RQ4-a**, we aimed to learn a reward function that explicitly prioritizes speed. To gather preference data, we first collected 56 time-trial trajectories generated by the default built-in AI (BIAI) agents, which are pre-programmed opponent drivers in the game. We then randomly sampled pairs of trajectories from this pool and labeled them according to their lap times. A shorter lap time is preferred, indicating faster driving. This process resulted in a total of 1429 preferences.

Next, for **RQ4-b**, our goal was to learn reward models for *aggressive* and *timid* driving styles in the versus task. Aggressive driving is characterized by frequent overtaking attempts, which may result in more collisions and off-track instances. In contrast, timid driving reflects a tendency to keep a distance from other cars, resulting in fewer car interactions and slower driving. To form the preference dataset, we trained RL

agents with slightly modified versions of the GT Sophy reward function [Wurman *et al.*, 2022] to induce different driving behaviors. We then collected 79 versus-task trajectories and organized them by car. For each car group, we expressed preferences—ranging from aggressive to timid—based on the behavioral indicators described above. This process resulted in 118 pairwise preferences. See Appendix C.1–C.2 for details on metrics and the preference collection process.

Training and Evaluation

We followed the same reward learning protocol and baseline comparisons described in Section 5.2, using Adam for optimization and a grid search for hyperparameter selection. Rather than fitting weights for all reward features, we restrict reward learning to the subset we believe to be most relevant to the behaviors reflected in the preference data. For **fast driving (RQ4-a)**, we consider the weight for the *progress* feature. This measures distance advanced along the track centerline; the primary driver of speed. For **aggressive/timid styles (RQ4-b)**, we consider the weights associated with the *overtaking* and *collision* features, as these are tied to interactive driving behaviors. All other reward weights remained fixed.

We performed the reward learning procedure across three seeds, and for each resulting reward model, we trained a new QR-SAC agent [Wurman *et al.*, 2022] on the Sarthe track. Note that although the preference data was collected from a subset of 19 cars, we train the policy to control all 552 cars in the game. For RQ4-a, training was done in the time-trial task, where a single car attempts to complete laps as quickly as possible. For RQ4-b, we trained with various versus tasks as described in Wurman *et al.* [2022] where the agent races against a range of opponents. Due to the high computational cost of GT7, we limited RL training to three seeds.

Next, to select policies for final evaluation, we periodically monitored performance during training and identified those policies that best optimized the metrics associated with the intended driving style (e.g., maximizing overtaking for aggressive agents). To ensure a fair comparison, this selection criterion was applied uniformly to all baselines. Selected policies were then evaluated across all 552 cars on Sarthe. For the fast driving experiments, evaluation was done in the time-trial task, where the agent completes a solo three-lap race, and the minimum lap time is recorded. We then report three metrics to assess performance: 1) BIAI ratio, defined as the RL agent’s lap time divided by the BIAI’s lap time for the same car (a BIAI ratio below 1.0 indicates that the agent is faster than the BIAI), 2) the minimal lap time (in seconds), and 3) the number of incomplete laps (i.e., lap time exceeds the maximum lap time of 1,800 seconds). For these metrics, lower is better. For the aggressive/timid experiments, we evaluate performance in a specific versus task, where the agent starts in last place and chases 19 BIAI opponents over a three-lap race (see Figure 14 in Appendix C.2 for an illustration). We measure the number of overtaking attempts, collisions, off-track instances, and the agent’s final position.

All metrics are first averaged across all 552 cars, then aggregated over the three seeds. We did not perform statistical testing for the GT7 experiments, as there are only three seeds, making such tests not meaningful. For further details

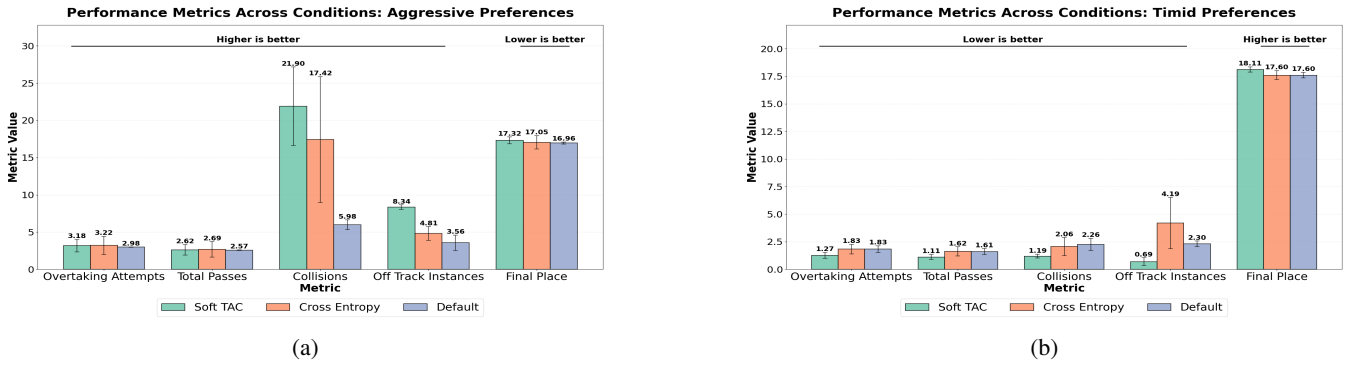


Figure 2: GT7 results for the versus tasks, illustrating how aggressive (a) or timid (b) each agent is (per the mean \pm SE of the four metrics) under different reward functions. For aggressive, higher metrics are better, and for timid, lower metrics are better (except for final place).

Table 2: BIAI ratio (\pm SE), minimal lap time (\pm SE), and number of incomplete laps after RL training with each reward (lower is better) in the GT7 time-trial task.

Method	BIAI Ratio	Lap Time	Incomplete Laps
SOFT-TAC	0.968 ± 0.01	269.96 ± 0.24	2
CROSS-ENTROPY	0.994 ± 0.01	277.45 ± 0.45	38
DEFAULT	0.989 ± 0.01	275.69 ± 0.33	18

on training and evaluation, see Appendix D.

Results: Controlling Fast Driving Styles

Our goal was to learn the progress reward weight such that the resulting RL-trained policy minimizes lap time in a time-trial task. In the default reward function, the weight for progress is 1.0, while Cross-Entropy and Soft-TAC learned a weight of ~ 0.5 and ~ 7.0 , respectively. This difference stems from how the losses handled a subset of misclassified preferences. Under Cross-Entropy, large gradients from these errors offset the gradients from the correctly classified points, resulting in a net gradient near zero that led the weight to plateau. Conversely, Soft-TAC suppressed the gradients of these errors toward zero, leaving only the signal from the correct data to drive the weight upward (see Appendix B.5). As shown in Table 2, Soft-TAC’s learned reward weights substantially improved performance, achieving the lowest BIAI ratio as well as reducing the average lap time by 7 seconds relative to Cross-Entropy and 5.5 seconds relative to the default reward. The reported averages exclude incomplete laps (lap time exceeds 1,800 seconds). Soft-TAC had only two such instances, far fewer than the other baselines.

Results: Controlling Aggressive and Timid Behavior

In these experiments, we controlled the overtaking and collision reward weights to produce both aggressive and timid driving behaviors while racing against opponents. The default reward function assigns an equal weight of 0.5 to both overtaking and collision. In the aggressive preference experiments, reward models trained with both Soft-TAC and Cross-

Entropy learned collision weights of ~ 0 , meaning the agent received no penalty for making contact with other cars. However, the Soft-TAC reward model learned a larger overtaking weight (~ 2.7) than both Cross-Entropy (~ 1.4) and the default reward function (0.5). As shown in Figure 2a, this resulted in RL policies trained with Soft-TAC reward models to exhibit more aggressive behavior. While the number of overtaking attempts was similar across methods, Soft-TAC agents produced more collisions and off-track events. Collisions indicate that the agent is driving close to other cars, whereas off-track events suggest attempts to gain an advantage by cutting corners. Importantly, this aggressive behavior did not negatively affect the agent’s final place. A similar pattern holds in the timid preference condition (see Figure 2b). In this case, Soft-TAC learned a higher collision penalty (~ 2.4) than both Cross-Entropy (~ 0.8) and the default reward (0.5), along with an overtaking weight of 0. These weights yielded behavior that was more timid than the baselines: Soft-TAC agents generated fewer overtaking attempts, collisions, and off-track events. See Figure 15 in Appendix C.1 for examples of aggressive and timid driving behaviors from policies trained with Soft-TAC learned reward models. Together, these results show that Soft-TAC can be used to learn preference-specific reward weights to produce clearly distinct timid and aggressive behaviors.

6 Conclusion

Designing effective reward functions is challenging, motivating our investigation into tools that better support this process. In a human-subject study, we found that TAC meaningfully assists RL practitioners in specifying reward weights: participants using TAC produced more performant reward functions while experiencing lower cognitive workload. However, the study also highlighted that manual tuning, even with TAC, remains labor-intensive, underscoring the need for automated approaches. To this end, we introduce Soft-TAC, a differentiable approximation used to train reward models so they agree as closely as possible with human preferences. In evaluations in GT7, Soft-TAC learned reward models that more accurately captured underlying preference-objectives than competing baselines. Overall, our findings show that TAC can serve as both a tool for reward tun-

ing and as an optimization objective for reward learning. While promising, our work focuses on linear reward functions, which assume access to a representative set of reward features. This constraint motivates two directions for future research: evaluating Soft-TAC with black-box reward models, and exploring whether TAC can help practitioners identify missing or informative reward features.

References

Dario Amodei, Chris Olah, Jacob Steinhardt, Paul Christiano, John Schulman, and Dan Mané. Concrete Problems in AI Safety. *CoRR, abs/1606.06565*, 2016.

Serena Booth, W. Bradley Knox, Julie Shah, Scott Niekum, Peter Stone, and Alessandro Allievi. The Perils of Trial-and-Error Reward Design: Mismatch through Overfitting and Invalid Task Specifications. In *AAAI Conference on Artificial Intelligence*, 2023.

Ralph Allan Bradley and Milton E. Terry. Rank Analysis of Incomplete Block Designs: I. The Method of Paired Comparisons. *Biometrika*, 1952.

Greg Brockman, Vicki Cheung, Ludwig Pettersson, Jonas Schneider, John Schulman, Jie Tang, and Wojciech Zaremba. OpenAI Gym, 2016.

Daniel S. Brown, Jordan Schneider, and Scott Niekum. Value Alignment Verification. In *International Conference on Machine Learning*, 2021.

Erdem Biyik and Dorsa Sadigh. Batch Active Preference-Based Learning of Reward Functions. In *Conference on Robot Learning*, 2018.

Jie Cheng, Gang Xiong, Xingyuan Dai, Qinghai Miao, Yisheng Lv, and Fei-Yue Wang. RIME: Robust Preference-based Reinforcement Learning with Noisy Preferences. In *International Conference on Machine Learning*, 2024.

Heewoong Choi, Sangwon Jung, Hongjoon Ahn, and Taesup Moon. Listwise Reward Estimation for Offline Preference-based Reinforcement Learning. In *International Conference on Machine Learning*, 2024.

Paul F Christiano, Jan Leike, Tom B Brown, Miljan Martic, Shane Legg, and Dario Amodei. Deep Reinforcement Learning from Human Preferences. In *Conference on Neural Information Processing Systems*, 2017.

Aritra Ghosh, Himanshu Kumar, and P. S. Sastry. Robust Loss Functions under Label Noise for Deep Neural Networks. In *AAAI Conference on Artificial Intelligence*, 2017.

Adam Gleave, Michael Dennis, Shane Legg, Stuart Russell, and Jan Leike. Quantifying Differences in Reward Functions. In *International Conference on Learning Representations*, 2021.

Tuomas Haarnoja, Aurick Zhou, Pieter Abbeel, and Sergey Levine. Soft Actor-Critic: Off-Policy Maximum Entropy Deep Reinforcement Learning with a Stochastic Actor. In *International Conference on Machine Learning*, 2018.

Sandra G. Hart and Lowell E. Staveland. Development of NASA-TLX (Task Load Index): Results of Empirical and Theoretical Research. *Advances in Psychology*, 52:139–183, 1988.

Joey Hejna, Rafael Rafailov, Harshit Sikchi, Chelsea Finn, Scott Niekum, W. Bradley Knox, and Dorsa Sadigh. Contrastive Preference Learning: Learning from Human Feedback Without RL. In *International Conference on Learning Representations*, 2024.

Donald Joseph Hejna III and Dorsa Sadigh. Few-Shot Preference Learning for Human-in-the-Loop RL. In *Conference on Robot Learning*, 2023.

Xiao Hu, Jianxiong Li, Xianyuan Zhan, Qing-Shan Jia, and Ya-Qin Zhang. Query-Policy Misalignment in Preference-Based Reinforcement Learning. In *International Conference on Learning Representations*, 2024.

Minyoung Hwang, Gunmin Lee, Hogun Kee, Chan Woo Kim, Kyungjae Lee, and Songhwai Oh. Sequential Preference Ranking for Efficient Reinforcement Learning from Human Feedback. In *Conference on Neural Information Processing Systems*, 2023.

Borja Ibarz, Jan Leike, Tobias Pohlen, Geoffrey Irving, Shane Legg, and Dario Amodei. Reward learning from Human Preferences and Demonstrations in Atari. In *Conference on Neural Information Processing Systems*, 2018.

Hyungkyu Kang and Min-hwan Oh. Adversarial Policy Optimization for Offline Preference-Based Reinforcement Learning. In *International Conference on Learning Representations*, 2025.

Maurice George Kendall. The Treatment of Ties in Ranking Problems. *Biometrika*, 33:239–251, 1945.

Diederik P. Kingma and Jimmy Lei Ba. Adam: A Method for Stochastic Optimization. In *International Conference on Learning Representations*, 2015.

W. Bradley Knox and James MacGlashan. How to Specify Reinforcement Learning Objectives. In *Finding the Frame: An RLC Workshop for Examining Conceptual Frameworks at the Reinforcement Learning Conference*, 2024.

W. Bradley Knox, Alessandro Allievi, Holger Banzhaf, Felix Schmitt, and Peter Stone. Reward (Mis)design for Autonomous Driving. *Artificial Intelligence*, 316(103829), 2023.

W. Bradley Knox, Stephane Hatgis-Kessell, Serena Booth, Scott Niekum, Peter Stone, and Alessandro G. Allievi. Models of Human Preference for Learning Reward Functions. *Transactions on Machine Learning Research*, 2024.

Kimin Lee, Laura Smith, and Pieter Abbeel. PEBBLE: Feedback-Efficient Interactive Reinforcement Learning via Relabeling Experience and Unsupervised Pre-training. In *International Conference on Machine Learning*, 2021.

Xinran Liang, Katherine Shu, Kimin Lee, and Pieter Abbeel. Reward Uncertainty for Exploration in Preference-based Reinforcement Learning. In *International Conference on Learning Representations*, 2022.

Runze Liu, Fengshuo Bai, Yali Du, and Yaodong Yang. Meta-Reward-Net: Implicitly Differentiable Reward Learning for Preference-based Reinforcement Learning. In *Conference on Neural Information Processing Systems*, 2022.

Calarina Muslimani and Matthew E Taylor. Leveraging Sub-Optimal Data for Human-in-the-Loop Reinforcement Learning. In *International Conference on Learning Representations*, 2025.

Calarina Muslimani, Kerrick Johnstonbaugh, Suyog Chandramouli, Serena Booth, W Bradley Knox, and Matthew E Taylor. Towards Improving Reward Design in RL: A Reward Alignment Metric for RL Practitioners. In *Reinforcement Learning Conference*, 2025.

Alizée Pace, Bernhard Schölkopf, Gunnar Rätsch, and Giorgia Ramponi. Preference Elicitation for Offline Reinforcement Learning. In *International Conference on Learning Representations*, 2025. ICLR 2025.

Jongjin Park, Younggyo Seo, Jinwoo Shin, Honglak Lee, Pieter Abbeel, and Kimin Lee. SURF: Semi-supervised Reward Learning with Data Augmentation for Feedback-efficient Preference-based Reinforcement Learning. In *International Conference on Learning Representations*, 2022.

Daniel Shin, Anca Dragan, and Daniel S. Brown. Benchmarks and Algorithms for Offline Preference-Based Reward Learning. *Transactions on Machine Learning Research*, 2023.

Joar Skalse, Nikolaus Howe, Dmitrii Krasheninnikov, and David Krueger. Defining and Characterizing Reward Gaming. In *Conference on Neural Information Processing Systems*, 2022.

Joar Max Viktor Skalse, Lucy Farnik, Sumeet Ramesh Motwani, Erik Jenner, Adam Gleave, and Alessandro Abate. STARC: A General Framework For Quantifying Differences Between Reward Functions. In *International Conference on Learning Representations*, 2024.

Hao Sun, Yunyi Shen, and Jean-Francois Ton. Rethinking Reward Modeling in Preference-based Large Language Model Alignment. In *International Conference on Learning Representations*, 2025.

Richard S Sutton and Andrew G Barto. *Reinforcement Learning: An Introduction*. MIT press, 2018.

Mudit Verma and Katherine Metcalf. Hindsight PRIORs for Reward Learning from Human Preferences. In *International Conference on Learning Representations*, 2024.

Blake Wulfe, Ashwin Balakrishna, Logan Ellis, Jean Mercat, Rowan McAllister, and Adrien Gaidon. Dynamics-Aware Comparison of Learned Reward Functions. In *International Conference on Learning Representations*, 2022.

Peter R. Wurman, Sam Barrett, Kei Kawamoto, James MacGlashan, Kaushik Subramanian, Thomas J. Walsh, Ryan Capobianco, Adnan Devlic, Florian Eckert, Frank Fuchs, et al. Outracing Champion Gran Turismo Drivers with Deep Reinforcement Learning. *Nature*, 602(7896):223–228, 2022.

Zhixian Xie, Haode Zhang, Yizhe Feng, and Wanxin Jin. Robust Reward Alignment via Hypothesis Space Batch Cutting. In *International Conference on Machine Learning*, 2025.

Kaipeng Zheng, Huishuai Zhang, and Weiran Huang. Dif-Kendall: A Novel Approach for Few-Shot Learning with Differentiable Kendall’s Rank Correlation. In *Conference on Neural Information Processing Systems*, 2023.

7 Ethical Statement

Our human-subject reward design study was approved by the relevant institutional ethics board, and all data were collected in accordance with ethical guidelines. All participants were informed about the study and provided consent prior to participation. We also introduce a new loss function for preference-based reward learning. When using such methods, it is important to ensure that the collected preferences are representative of the target population to avoid introducing bias into deployed models.

Appendix

A User Study Details

A.1 Environment: Lunar Lander

In the Lunar Lander environment, the agent begins near the top-center of the screen and must land on a fixed landing pad as quickly and smoothly as possible, avoiding excessive hovering or unstable movements. The agent selects actions from a 2-dimensional continuous space controlling the main engine thrust and the side engines for lateral movement. The state space is an 8-dimensional vector containing position, velocity, angle, angular velocity, and two leg-contact indicators. An episode ends when the lander crashes, goes off screen, or comes to rest—either due to a successful landing or because it has stopped moving.

Reward Function Components

The agent receives a reward defined as a linear combination of eight features. Below we describe each component used in the Lunar Lander reward function.

1. Progress-based rewards

- **Progress toward the landing pad.** Measures the change in Euclidean distance between the lander and the landing pad across consecutive time steps. A negative weight rewards the agent for reducing this distance (moving closer).
- **Change in lander speed.** Measures the change in the lander’s velocity magnitude. A positive weight rewards acceleration, while a negative weight rewards deceleration.
- **Change in lander angle (uprightness).** Measures changes in the absolute tilt angle. A negative weight rewards the lander for becoming more upright.
- **Change in leg contact.** Measures differences in the number of legs in contact with the ground (0–2) between steps. A positive weight rewards gaining contact, while a negative weight rewards losing contact.

2. Absolute rewards

- **Side engine use.** A binary reward indicating whether the side engine is activated in the current step. A positive weight encourages more usage; a negative weight discourages it.
- **Main engine use.** A binary reward indicating whether the main engine is being used. Positive weights encourage usage; negative weights discourage it.
- **Crashing.** A binary reward indicating whether the lander crashes. Negative weights penalize crashes, whereas positive weights encourage them.
- **Safe landing.** A binary reward indicating when the lander completes a safe landing. Positive weights encourage successful landings; negative weights discourage them.

A.2 User Study Interface

In Figures 3–8, we present images of the Jupyter notebook interface used in the human-subject study.

Task 0: Loading the notebook

To run a cell, click on the play button (triangle icon).

Do not load all the cells at once, as this can cause issues in the notebook loading properly.

The first cell below can take up to 5 minutes to load, as it is loading trajectories and videos. There are progress bars to show you how much time is left.

Please wait for the cell to complete before proceeding to the next sections.

```
[1]: # import notebooks; do not edit, will take approximately 5 minutes to load
import backend
interface = backend.interface_backend()
```

Figure 3: Image of user study: Task 0 – Loading the notebook

Task 1: Understanding the Domain: Lunar Lander

Objective

In Lunar Lander, the agent is initialized at a random location near the top-center of the screen. The task is to land on a fixed landing pad both quickly and smoothly, discouraging excessive hovering, jittering, or unstable movements.

Action Space

The action is a 2-dimensional vector consisting of:

- The first value controls the main engine throttle (up/down arrow).
- The second value controls the side engines, which move the lander left or right.

Observation Space

The state is an 8-dimensional vector consisting of:

- The lander’s x-coordinate, y-coordinate
- The lander’s x-velocity, y-velocity
- The lander’s angle and angular velocity
- 2 booleans that represent whether each leg is in contact with the ground or not.

Episode Termination

The episode ends if:

- The lander crashes.
- The lander goes off screen.
- The lander is not moving. This includes when the agent successfully lands on the landing pad.

Watch the videos below to see an example of a successful lunar lander agent (left) and a failing lunar lander agent (right)



Figure 4: Image of user study: Task 1 – Reviewing the domain

Task 2: Understanding the Domain Expert’s Preferences

Imagine you’re working alongside a *domain expert* in the Lunar-Lander environment. The domain expert has spent a lot of time and effort observing the agent’s behavior and carefully provided pairwise preferences for a set of trajectories. However, while the expert knows how to judge the degree of task success, they *cannot define a reward function themselves*.

As someone with RL experience, your job in this task is to *watch the video clips, review the preferences, and understand what the expert values most in agent behavior*. We provided pairwise preferences for 15 video clips.

This understanding will be important for your next step.

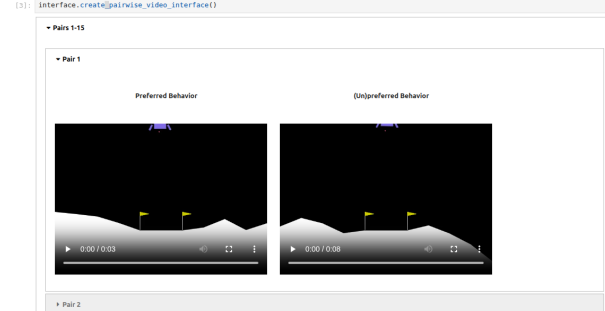


Figure 5: Image of user study: Task 2 – Reviewing the domain expert’s preferences

Task 3: Choosing the Best Reward Function

```
[4]: interface.show_reward_structure()
```

Review of Reward Function Components

The agent receives a linear combination of the following 8 different features. Here's what each reward component measures:

Progress-based rewards

- **Progress toward the landing pad.** Measures the change in Euclidean distance from the lander's position (`x_pos`, `y_pos`) to the landing pad between consecutive steps. Positive weight rewards the lander for increasing its distance from the pad, while a negative weight rewards it for decreasing the distance (getting closer). [Show reward code](#)
- **Change in lander speed.** Measures the change in the lander's velocity (`x_vel`, `y_vel`) between consecutive steps. Positive weight rewards the lander for accelerating (increasing its speed), while a negative weight rewards it for decelerating (slowing down). [Show reward code](#)
- **Change in lander angle (uprightness).** Measures the change in the lander's tilt (`angle`) between consecutive steps. Positive weight rewards the lander for more, while a negative weight rewards it for becoming more upright. [Show reward code](#)
- **Change in leg contact with the ground.** Measures whether the lander is gaining or losing leg contact with the ground between steps. Each leg contact is binary (0 = no contact, 1 = contact). Positive weight rewards the lander for gaining more leg contact, while a negative weight rewards it for losing contact. [Show reward code](#)

Absolute rewards

- **Side engine use.** Provides a binary reward when the lander uses its side engine at the current time step. Positive weight encourages more use, negative weight encourages less. [Show reward code](#)
- **Main engine use.** Provides a binary reward when the lander uses its main engine at the current time step. Positive weight encourages more use, negative weight encourages less. [Show reward code](#)
- **Crashing.** Provides a binary reward when the lander crashes at the current time step. Positive weight encourages more crashes, negative weight encourages fewer. [Show reward code](#)
- **Safe landing.** Provides a binary reward when the lander achieves a safe landing at the current time step. Positive weight encourages more safe landings, negative weight encourages fewer. [Show reward code](#)

Figure 6: Image of user study: Task 3, Part A – Reviewing the Lunar Lander reward parts

```
[5]: interface.get_task_instructions()
```

Your Task as an RL Practitioner

Your goal is to select the reward function that best captures what the **expert values**. Since the domain expert cannot directly define a reward function, they are relying on you to translate their preferences into a meaningful reward function that teaches the agent to behave as they expect.

Recall that the agent's reward is a linear combination of the 8 reward features described above. **It is your task to select the weights for each of these 8 reward features.** You can choose any positive or negative value.

Alignment Feedback:

To help you select the reward weights:

1. You will be provided with a reward alignment score that indicates how well your reward function encodes the domain expert's preferences. It is a score from 1 (best case) to -1 (worst case). An alignment score close to 1 indicates that the reward function induces **similar preferences as the domain expert!** An alignment score close to -1 indicates that the reward function induces **opposite preferences as the domain expert!** Note that the alignment score is computed with the preferences shown in the video, and an additional set of preferences from the same domain expert.
2. You can rewatch the videos from task 1 to remind you of what the domain expert prefers in agent behavior.
3. For each of the video pairs, we will also provide the return under the new reward function you selected. This can help you understand how your chosen weights affect the evaluation of different agent behaviors.

You can submit multiple weight configurations, but once you are done, **the most recent submissions will be used as the final weights.** We will then use your reward function to train an RL agent with discount factor $\gamma = 0.99$.

Figure 7: Image of user study: Task 3, Part B – Reviewing the reward tuning instructions

```
[6]: results = interface.select_reward_weights()
```

Enter Reward Function Weights

lunar_distance_reward:	0
lunar_speed_reward:	0
lunar_tilt_reward:	0
lunar_leg_contact_reward:	0
lunar_side_engine_reward:	0
lunar_main_engine_reward:	0
lunar_crash_reward:	0
lunar_safe_landing_reward:	-100

Submit Weights & Get Alignment

```
*** Submission #1 ***
Time: 2025-12-18 18:38:14
Height: 1000.0
lunar_distance_reward: 0.0
lunar_speed_reward: 0.0
lunar_tilt_reward: 0.0
lunar_leg_contact_reward: 0.0
lunar_side_engine_reward: 0.0
lunar_main_engine_reward: 0.0
lunar_crash_reward: 0.0
lunar_safe_landing_reward: -100.0

Calculating alignment...
Alignment Result: -0.7632031385968296
NEW BEST SCORE!
```

Figure 8: Image of user study: Task 3, Part C – Reward tuning UI

A.3 Additional Results

In addition to the NASA-TLX survey, we also asked participants to rate their reward design experience on a 1–7 scale. Participants in the Alignment group reported slightly higher experience (mean = 5.83, SE = 0.31) than those in the Control group (mean = 4.8, SE = 0.86). However, this difference was not statistically significant according to a Welch's *t*-test ($t = -1.13$, $p = 0.15$). Thus, reward design experience is

unlikely to be a confounding factor.

Next, Table 3 summarizes the tuned reward functions provided by all participants. We find that 10 out of 11 participants opted for dense reward structures rather than sparse ones. The resulting reward weights also varied widely, especially for the distance, tilt, crash, and safe-landing components.

Table 3: Participant-tuned reward weights and resulting evaluation metrics (TAC, Average Landing-pad Success Rate, and number of reward tuning iterations).

Metric	P1	P2	P3	P4	P5	P6
CONTROL CONDITION						
<i>Reward Weights</i>						
Distance	-1.0	-0.4	-55.5	1.0	-2000.0	-
Speed	0.0	-0.5	0.0	1.0	-10.0	-
Tilt	-1.0	-0.4	0.0	0.0	-10.0	-
Leg Contact	1.0	0.0	10.0	1.0	0.0	-
Side Engine	-0.1	-0.25	5.0	0.05	-1.0	-
Main Engine	-0.1	-0.1	1.0	0.05	-1.0	-
Crash	-10.0	-2.0	20.0	-10.0	-1000.0	-
Safe Landing	10.0	100.0	100.0	10.0	1000.0	-
<i>Evaluation Metrics</i>						
TAC	0.68	0.61	0.24	0.41	0.64	-
Landing-pad Success Rate	0.0	0.0	0.0	0.0	0.992	-
Tuning Iterations	8	21	79	54	86	-
ALIGNMENT CONDITION						
<i>Reward Weights</i>						
Distance	-2.0	-1.0	3.0	0.0	-10.0	-100.0
Speed	-1.0	0.1	1.0	0.0	-2.5	-5.0
Tilt	-0.1	-0.1	-2.0	0.0	-1.5	-100.0
Leg Contact	1.0	1.0	4.0	0.0	1.5	1.0
Side Engine	-0.01	0.0	0.0	0.0	-0.1	0.0
Main Engine	-0.05	0.0	0.0	0.0	-0.05	0.0
Crash	-5.0	-10.0	-5.0	0.0	-25.0	-50.0
Safe Landing	1000.0	10.0	5.0	1000.0	78.0	10000.0
<i>Evaluation Metrics</i>						
TAC	0.75	0.62	0.42	0.73	0.76	0.81
Landing-pad Success Rate	0.6	1.0	0.0	0.168	1.0	0.992
Tuning Iterations	19	5	16	55	80	89

B Soft TAC Details

B.1 Discussion on the Lack of Human Preferences used in Preference Based RL

Despite the goal of learning reward functions from human preferences, most works in the literature assume access to an oracle environment reward function. As a result, it is not standard for PbRL algorithms to be evaluated with actual human preference data. Instead, these algorithms are commonly tested using synthetic preferences derived from the environment’s “ground truth” reward function. For example, the following works (not an exhaustive list) spanning 2018 to 2025 do not include any human experiments: Ibarz *et al.* [2018]; Liang *et al.* [2022]; Park *et al.* [2022]; Liu *et al.* [2022]; Shin *et al.* [2023]; Cheng *et al.* [2024]; Hu *et al.* [2024]; Verma and Metcalf [2024]; Choi *et al.* [2024]; Kang and Oh [2025]; Pace *et al.* [2025]. See Muslimani and Taylor [2025] for a more extensive survey of PbRL algorithms without human preferences. Our work uses human preference data, which distinguishes it from the current literature, and we encourage more work to consider using human preferences instead of synthetic.

B.2 Proof for Proposition 1

Proof. Let (τ^i, τ^j) be an arbitrary pair of trajectories with human preference label $y \in \{-1, 1\}$ (1 indicates $\tau^i \succ \tau^j$, and -1 otherwise) in the dataset \mathcal{D}_h . We assume there are no ties in \mathcal{D}_h (e.g., the label y cannot be 0). Next, we define the difference in predicted returns between trajectories τ^i and τ^j under the learned reward function \hat{r}_θ as:

$$\Delta G_r(\tau^i, \tau^j) \doteq \sum_t \hat{r}_\theta(s_t^i, a_t^i) - \sum_t \hat{r}_\theta(s_t^j, a_t^j),$$

We break the analysis into two cases:

Case 1: Concordant pair

This occurs when the difference in predicted returns agrees with the human preference (i.e., $\text{sign}(\Delta G_r(\tau^i, \tau^j)) = y$). There are two subcases:

- If $y = 1$ and $\Delta G_r(\tau^i, \tau^j) > 0$, then

$$\lim_{\alpha \rightarrow \infty} \tanh(\alpha \Delta G_r(\tau^i, \tau^j)) = 1,$$

$$\lim_{\alpha \rightarrow \infty} y \cdot \tanh(\alpha \Delta G_r(\tau^i, \tau^j)) = 1.$$

- If $y = -1$ and $\Delta G_r(\tau^i, \tau^j) < 0$, then

$$\lim_{\alpha \rightarrow \infty} \tanh(\alpha \Delta G_r(\tau^i, \tau^j)) = -1,$$

$$\lim_{\alpha \rightarrow \infty} y \cdot \tanh(\alpha \Delta G_r(\tau^i, \tau^j)) = 1.$$

Thus, for any concordant pair:

$$\lim_{\alpha \rightarrow \infty} y \cdot \tanh(\alpha \Delta G_r(\tau^i, \tau^j)) = 1.$$

Case 2: Discordant pair

This occurs when the difference in predicted returns disagrees with the human preference (i.e., $\text{sign}(\Delta G_r(\tau^i, \tau^j)) \neq y$). There are two subcases:

- If $y = 1$ and $\Delta G_r(\tau^i, \tau^j) < 0$, then

$$\lim_{\alpha \rightarrow \infty} \tanh(\alpha \Delta G_r(\tau^i, \tau^j)) = -1,$$

$$\lim_{\alpha \rightarrow \infty} y \cdot \tanh(\alpha \Delta G_r(\tau^i, \tau^j)) = -1.$$

- If $y = -1$ and $\Delta G_r(\tau^i, \tau^j) > 0$, then

$$\lim_{\alpha \rightarrow \infty} \tanh(\alpha \Delta G_r(\tau^i, \tau^j)) = 1,$$

$$\lim_{\alpha \rightarrow \infty} y \cdot \tanh(\alpha \Delta G_r(\tau^i, \tau^j)) = -1.$$

Hence, for any discordant pair:

$$\lim_{\alpha \rightarrow \infty} y \cdot \tanh(\alpha \Delta G_r(\tau^i, \tau^j)) = -1.$$

Combining all pairs:

Define P as the number of concordant pairs and Q as the number of discordant pairs, with $N = P+Q$ the total number of pairs. Then, using the results from Cases 1 and 2, we have

$$\begin{aligned} & \lim_{\alpha \rightarrow \infty} \tilde{\sigma}_{\text{TAC}}(\mathcal{D}_h, G_r) \\ &= \lim_{\alpha \rightarrow \infty} \mathbb{E}_{(\tau^i, \tau^j, y) \sim \mathcal{D}_h} \left[y \cdot \tanh(\alpha \Delta G_r(\tau^i, \tau^j)) \right] \\ &= \frac{1}{N} \sum_{(\tau^i, \tau^j, y) \in \mathcal{D}_h} \left[\lim_{\alpha \rightarrow \infty} y \cdot \tanh(\alpha \Delta G_r(\tau^i, \tau^j)) \right] \\ &= \frac{P - Q}{N} \\ &= \sigma_{\text{TAC}} \end{aligned}$$

□

B.3 Proof for Theorem 1

Proof. (\Leftarrow) Let $r_{\theta^*} \in \mathcal{R}_{\text{human}}$ provided by Assumption 2, then by Definition 2, given any arbitrary $(\tau^i, \tau^j, y) \in \mathcal{D}_h$:

$$y \cdot \Delta G_{r_{\theta^*}}(\tau^i, \tau^j) > 0$$

Then, the individual loss in the limit is:

$$\lim_{\alpha \rightarrow \infty} 1 - y \cdot \tanh(\alpha \Delta G_{r_{\theta^*}}(\tau^i, \tau^j)) = 1 - 1 = 0.$$

Averaging over \mathcal{D}_h , the total loss, $L_{\text{Soft-TAC}}(\theta^*; \mathcal{D}_h)$ is:

$$\begin{aligned} &= \lim_{\alpha \rightarrow \infty} \mathbb{E}_{(\tau^i, \tau^j, y) \sim \mathcal{D}_h} \left[1 - y \cdot \tanh(\alpha \Delta G_{r_{\theta^*}}(\tau^i, \tau^j)) \right] \\ &= \frac{1}{N} \sum_{(\tau^i, \tau^j, y) \in \mathcal{D}_h} \left[\lim_{\alpha \rightarrow \infty} 1 - y \cdot \tanh(\alpha \Delta G_{r_{\theta^*}}(\tau^i, \tau^j)) \right] \\ &= \frac{1}{N} \sum_{(\tau^i, \tau^j, y) \in \mathcal{D}_h} (1 - 1) = 0. \end{aligned}$$

Since the loss $1 - y \cdot \tanh(\cdot)$ is bounded below by 0, and we have achieved this bound, r_{θ^*} is a global minimizer.

(\implies) Suppose, for the sake of contradiction, that r_{θ^*} is a global minimizer of $\mathcal{L}_{\text{Soft-TAC}}(\theta; \mathcal{D}_h)$ such that $\mathcal{L}_{\text{Soft-TAC}}(\theta^*; \mathcal{D}_h) = 0$, but $r_{\theta^*} \notin \mathcal{R}_{\text{human}}$. Then, by the definition of $\mathcal{R}_{\text{human}}$, there must exist at least one triplet $(\tau^i, \tau^j, y) \in \mathcal{D}_h$ such that $y \cdot \Delta G_{r_{\theta^*}}(\tau^i, \tau^j) \leq 0$.

1. **Case 1: Opposite Sign.** If $y \cdot \Delta G_{r_{\theta^*}}(\tau^i, \tau^j) < 0$, then in the limit, the individual loss, $\ell_{i,j}$ for (τ^i, τ^j, y) is:

$$\lim_{\alpha \rightarrow \infty} 1 - y \cdot \tanh(\alpha \Delta G_{r_{\theta^*}}(\tau^i, \tau^j)) = 1 - (-1) = 2.$$

2. **Case 2: Zero Difference.** Similarly, if $y \cdot \Delta G_{r_{\theta^*}}(\tau^i, \tau^j) = 0$, then in the limit $\ell_{i,j}$ is:

$$\lim_{\alpha \rightarrow \infty} 1 - y \cdot \tanh(\alpha \Delta G_{r_{\theta^*}}(\tau^i, \tau^j)) = 1 - (0) = 1.$$

We let $\ell_{i,j}$ denote the individual loss incurred from the trajectory pair (τ^i, τ^j) and its associated label y . In both **case 1 and 2**, $\ell_{i,j} > 0$. Next, we note that the individual loss for any $(\tau^n, \tau^m, y) \in \mathcal{D}_h$ is non-negative ($\ell_{m,n} \geq 0$). Therefore, the total loss in the limit is:

$$\begin{aligned} \mathcal{L}_{\text{Soft-TAC}}(\theta^*; \mathcal{D}_h) &= \frac{1}{N} \left(\ell_{i,j} + \sum_{(m,n) \neq (i,j)} \ell_{m,n} \right) \\ &\geq \frac{1}{N} (\ell_{i,j} + 0) \\ &> 0. \end{aligned} \tag{6}$$

This contradicts the premise r_{θ^*} is a global minimizer of $\mathcal{L}_{\text{Soft-TAC}}(\theta; \mathcal{D}_h)$, meaning the loss is 0. Thus, r_{θ^*} must be in $\mathcal{R}_{\text{human}}$. □

B.4 Proof for Theorem 2

Ghosh *et al.* [2017] establish that a loss function can be *noise-tolerant* under simple non-uniform label noise, where labels are flipped with probability $\eta_{\mathbf{x}}$ that depends on the input \mathbf{x} . Their result implies that, for classification with n classes, noise tolerance is guaranteed provided that

$$\eta_{\mathbf{x}} < \frac{n-1}{n} \quad \text{for all } \mathbf{x} \in \mathcal{X},$$

if the loss function satisfies the following two conditions:

1. **Symmetry Condition:** $\sum_{y \in \{-1, 0, 1\}} L(f(x), y) = C, \forall x \in \mathcal{X}, \forall f$, where y is the class label and C is a constant.
2. **Zero Risk:** The global minimum expected risk on clean data is zero, $R_L(f^*) = 0$.

Therefore, it is only necessary to show that Soft-TAC satisfies these conditions. First, we establish that Soft-TAC is symmetric.

Proof. Consider the loss function $L(z, y)$ where $z \in \mathbb{R}$ is a scalar prediction and $y \in \{-1, 0, 1\}$ is the class label. For

any arbitrary scalar z (representing the model output $f(x)$ for any f), the sum over the labels is:

$$\begin{aligned} \sum_{y \in \{-1, 0, 1\}} L(z, y) &= [1 - \tanh(\alpha z)] + [1 + \tanh(\alpha z)] + 1 \\ &= 1 + 1 + 1 = 3. \end{aligned}$$

In our specific setting, the prediction z is given by the reward difference between (τ^i, τ^j) . In particular, $z = f(x) = \Delta G_{r_\theta}(\tau^i, \tau^j)$ under the reward model r_θ . Since the sum equals a constant ($C = 3$) for any scalar input $z = f(x)$, the symmetry condition is satisfied $\forall x \in \mathcal{X}$ and $\forall f$. \square

Next, we show that the expected risk for the global minimizer of Soft-TAC is 0. We first start with a few definitions.

Definition 3. Let $\mathcal{D}_h^{\text{pop}}$ denote the (unknown) probability distribution over preference tuples (τ^i, τ^j, y) from which the dataset $\mathcal{D}_h = \{(\tau^i, \tau^j, y)\}_N$ is sampled i.i.d.

Definition 4. Let $\mathcal{R}_{\text{human}}^{\text{pop}}$ be the set of reward functions r such that

$$\mathbb{P}_{(\tau^i, \tau^j, y) \sim \mathcal{D}_h^{\text{pop}}} \left[y \cdot (G_r(\tau^i) - G_r(\tau^j)) > 0 \right] = 1.$$

Proof. Let $r_{\theta^*} \in \mathcal{R}_{\text{human}}^{\text{pop}}$. By Definition 4, for $(\tau^i, \tau^j, y) \sim \mathcal{D}_h^{\text{pop}}$, we have

$$y \cdot \Delta G_{r_{\theta^*}}(\tau^i, \tau^j) > 0 \quad \text{with probability 1.}$$

Then, the per-sample Soft-TAC loss satisfies

$$\begin{aligned} \lim_{\alpha \rightarrow \infty} \ell_{i,j} &:= \lim_{\alpha \rightarrow \infty} [1 - y \cdot \tanh(\alpha \Delta G_{r_{\theta^*}}(\tau^i, \tau^j))] \\ &= 0. \end{aligned}$$

Moreover, the loss is uniformly bounded:

$$0 \leq \ell_{i,j} \leq 2 \quad \text{for all } \alpha, (\tau^i, \tau^j, y).$$

Now we apply the dominated convergence theorem (DCT):

$$\begin{aligned} \lim_{\alpha \rightarrow \infty} \mathcal{L}_{\text{Soft-TAC}}(\theta^*; \mathcal{D}_h^{\text{pop}}) &= \lim_{\alpha \rightarrow \infty} \mathbb{E}_{(\tau^i, \tau^j, y) \sim \mathcal{D}_h^{\text{pop}}} [\ell_{i,j}] \\ &\stackrel{\text{DCT}}{=} \mathbb{E}_{(\tau^i, \tau^j, y) \sim \mathcal{D}_h^{\text{pop}}} \left[\lim_{\alpha \rightarrow \infty} \ell_{i,j} \right] \\ &= \mathbb{E}_{(\tau^i, \tau^j, y) \sim \mathcal{D}_h^{\text{pop}}} [0] \\ &= 0. \end{aligned}$$

Thus, the expected Soft-TAC risk is zero in the limit $\alpha \rightarrow \infty$. \square

B.5 Understanding the Gradient Behavior of Soft-TAC versus Cross-Entropy

In Section 5.1, we discuss that the gradient of Soft-TAC goes to zero for data points where the prediction is confidently incorrect, whereas the gradient of Cross-Entropy does not. However, we note that this can be a positive attribute in cases where the dataset contains noisy or incorrect labels. We show that this phenomenon occurs in a toy supervised learning example.

In our toy preference-learning example, we learn a linear reward function from pairwise comparisons. We consider five

items with feature values $\phi_0 = 0, \phi_1 = 1, \phi_2 = 2, \phi_3 = 3$, and $\phi_4 = 4$, and aim to learn a single scalar weight w defining a linear reward function $r(\phi_i) = w\phi_i$, such that the induced reward ordering is consistent with the observed preferences.

The training dataset consists of five pairwise comparisons: $(0, 1, -1)$, $(1, 2, -1)$, $(2, 3, -1)$, $(3, 4, -1)$, and $(2, 4, +1)$. Each triplet (ϕ_i, ϕ_j, y) denotes a comparison, where $y = -1$ indicates that the item with feature ϕ_i is preferred over the item with feature ϕ_j , and $y = +1$ indicates the opposite. In all but one comparison, the item with the higher feature value is preferred. The comparison $(2, 4, +1)$ therefore represents an incorrectly labeled data point, modeling the presence of noisy preference labels in the dataset.

We perform supervised learning using stochastic gradient descent with the Adam optimizer, a learning rate of 0.1, and 40 training epochs. We use SGD to explicitly examine how correctly and incorrectly labeled data points influence the gradient and, consequently, the weight updates. We compare two loss functions: Soft-TAC and the standard Cross-Entropy.

As shown in Figure 9a, the gradient of the Soft-TAC objective for the incorrectly labeled data point decays toward zero, with a final magnitude of approximately 6×10^{-4} . In contrast, the gradients for the correctly labeled data points converge to values around 0.035. This behavior results in a monotonic increase in the learned weight, which reaches a final value of approximately 2.3, as shown in Figure 9b.

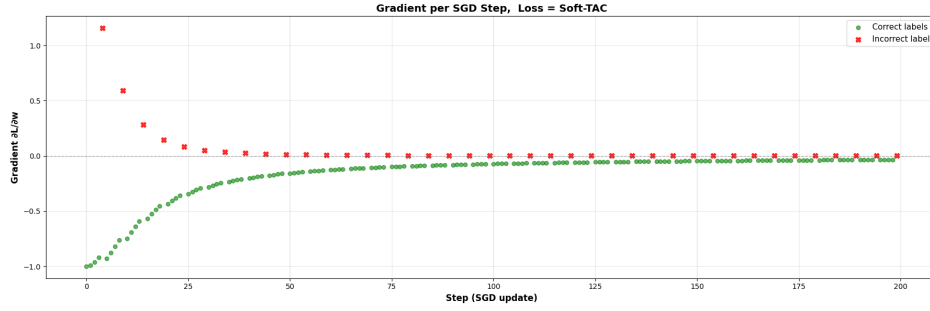
By comparison, Figure 10a shows that under the Cross-Entropy loss, the gradient for the incorrectly labeled data point remains large, persisting at approximately 1.5 throughout training, while gradients for the correctly labeled data points remain in the range of -0.3 to -0.4 . These conflicting gradients lead to unstable weight updates: although updates from correctly labeled data increase the weight, a single update from the incorrectly labeled data point substantially decreases it, undoing much of the accumulated progress. As a result, the weight increases only marginally over training, as shown in Figure 10b.

Overall, this toy example illustrates how Soft-TAC naturally downweights inconsistent or noisy preference labels by driving their gradients toward zero, whereas Cross-Entropy continues to enforce large gradients on mislabeled comparisons, hindering stable reward learning. In the absence of label noise, both loss functions recover a reward that induces the correct preference ordering in this toy setting (see Figures 11 and 12).

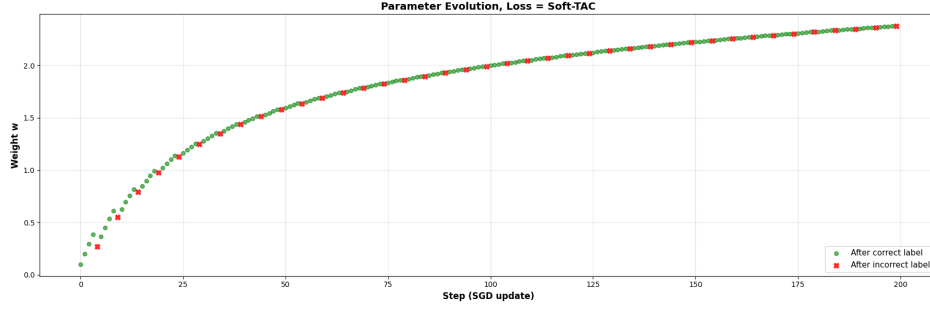
C Environment Details

C.1 Gran Turismo 7

GT7 is a high-fidelity racing simulator with multiple racing tracks, racing cars, and racing tasks. The agent's action space is 2-dimensional, with the agent controlling a car's velocity (e.g., accelerating or breaking) and steering input (e.g., turning left or right). The agent's state space consists of a variety of relevant features, such as an encoded static map of the track, its current position, velocity, and acceleration, as well as those of other opponents. For a complete description of the GT7 environment, see Wurman *et al.* [2022]. The code for GT7 is proprietary.

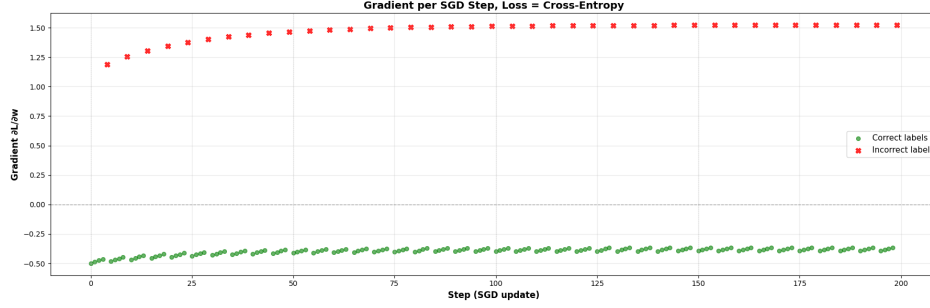


(a) Gradient behavior per SGD step.

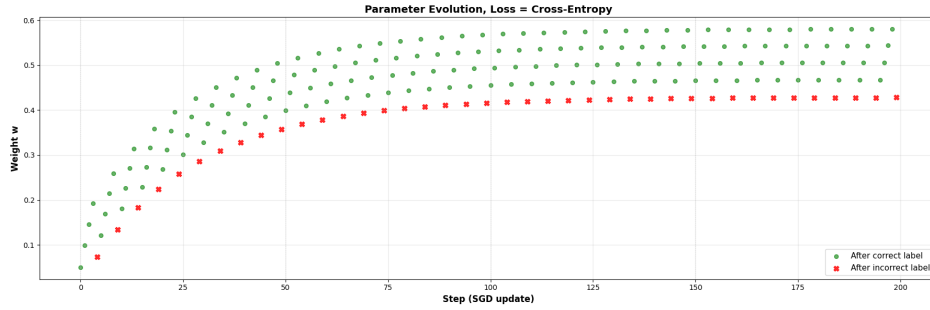


(b) Parameter evolution showing impact of each label type.

Figure 9: Soft-TAC loss behavior in a simple toy preference learning example with **noisy** data.



(a) Gradient behavior per SGD step.



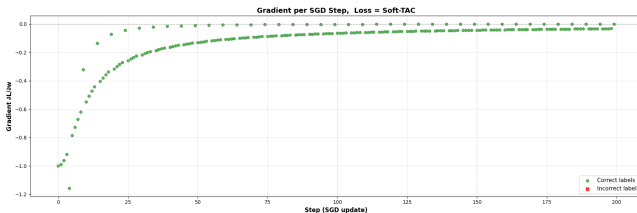
(b) Parameter evolution showing impact of each label type.

Figure 10: Cross-entropy loss behavior in a simple toy preference learning example with **noisy** data.

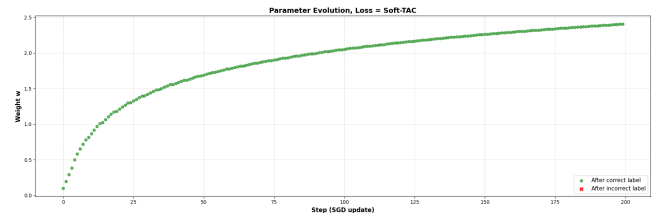
GT7 Cars used in Preference Dataset

In all GT7 experiments, we selected a subset of 19 cars to collect our preference dataset; it is not computationally feasible

to collect data for all 552 cars available in GT7. These cars were chosen uniformly with respect to Performance Points (PP) to ensure good coverage across the full range of PP values.

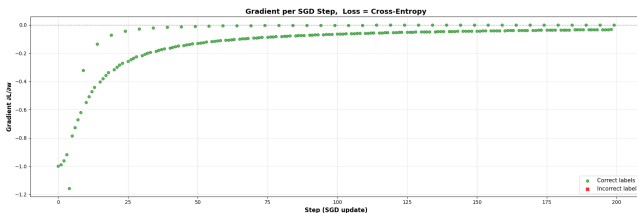


(a) Gradient behavior per SGD step.

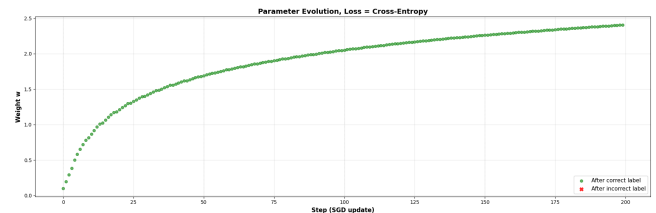


(b) Parameter evolution showing impact of each label type.

Figure 11: Soft-TAC loss behavior in a simple toy preference learning example with **noise-free** data.



(a) Gradient behavior per SGD step.



(b) Parameter evolution showing impact of each label type.

Figure 12: Cross-Entropy loss behavior in a simple toy preference learning example with **noise-free** data.

ues. PP is an in-game metric measuring car performance, where higher PP indicates a more powerful and faster car. This selection ensures that the trajectories capture a diverse set of driving behaviors and performance levels. As shown in Figure 13, the 19 selected cars provide broad PP coverage across the full set of cars.

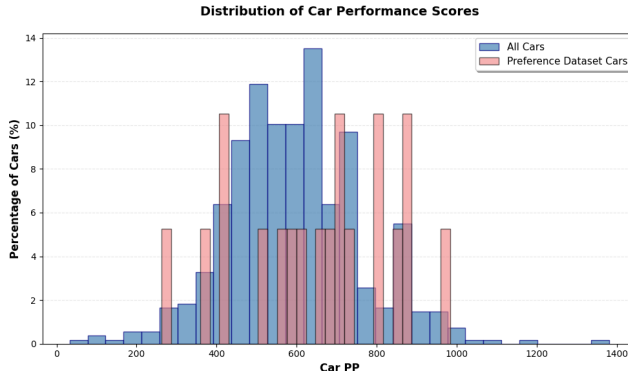


Figure 13: Distribution of Performance Points (PP) among all GT cars versus GT Cars in the preference dataset.

Reward Function Components

The reward function to train a GT7 agent was defined as a linear combination of different features, and the features differed based on whether the task was time-trial or versus. We describe only the reward features we learned for each task below, and in Table 4 we outline the specific weights for each reward feature used in the default (i.e., not learned) reward function. Other reward components are based on those described Wurman *et al.* [2022], along with a few additional parts that improved racing robustness.

1. Time-trial

- **Course Progress.** Measures the change in progress made along the track per step. More specifically, at each time step, we calculate the agent’s distance from the closest point on the track’s centerline. Then to calculate progress, we take the difference between the agent’s current and previous distances.

2. Versus Task

- **Velocity-based Collision Penalty.** This penalizes a car for colliding with another opponent and is based on the difference in velocity. More specifically, it is the squared difference in the car’s velocity and the opponent’s velocity at the time of the collision.
- **Overtaking.** This positively rewards the agent for overtaking opponents, but also penalizes the agent for being passed by an opponent. More specifically, we first find all opponents that are either 20 meters behind or 40 meters ahead of the agent. We refer to the set of these in-range opponents as $D_{opp-in-range}$. For each opponent $\in D_{opp-in-range}$, we calculate the change in the agent’s relative position along the track for each opponent from the previous time step to the current time step. The reward is then a sum over all these deltas.

Table 4: GT7 Default Reward Weights

Reward Part	Versus	Time-Trial
Course Progress	1.0	1.0
Velocity-based Collision	-0.5	NA
Passing	0.5	NA

In the fast driving experiments for the time-trial task (RQ4-a), we learned the weight for the course progress reward part. In the controlling aggressiveness/timidness experiments for the versus tasks (RQ4-b), we learned the velocity-based collision and overtaking reward weights.

Evaluation Metrics

The performance of the fast driving experiments in the time-trial task was evaluated by the three metrics described in Section 5.3, reported in Table 2: BIAI ratio, minimal lap time (in seconds), and the number of incomplete laps (i.e., lap time exceeds the maximum lap time of 1,800 seconds). For the controlling aggressive/timid experiments, we describe the evaluation metrics reported in Section 5.3, Figure 2.

- Collisions.** Evaluates the car’s velocity toward an opponent when a collision is detected. When this value exceeds a set threshold, the counter for the number of collisions increases.
- Overtaking Attempts.** We check for a sign change in the relative distance between consecutive time steps. A change from positive to negative indicates that the car has transitioned from being behind an opponent to being ahead in terms of forward progress along the track. If this sign change occurs while the car and its opponent are within 40 meters of each other, the event is classified as an overtaking attempt.
- Off Track Instances.** Tracks how many times the car has gone off the track by recording each instance when any of its four tires leave the track surface.
- Final Place.** Indicates the agent’s position rank at the end of the race out of 19 opponents. A final place of 0 refers to the first position, and 19 means the last.

C.2 Preference Collection Details

To collect trajectories for the aggressiveness/timidness experiments, we used two types of versus tasks in which the agent started in 20th place and chased 19 opponents over a three-lap race. The tasks differed in the type of opponent the agent raced against: (1) BIAI opponents and (2) copies of the agent itself (see Figure 14 for an illustration of the task setup).

Initially, we collected 45 trajectories and grouped them into nine sets of five, organized by car type and task type. Two trajectories were discarded from this initial set because the agent failed to complete the race, ensuring a high-quality dataset. Among the retained trajectories, four sets of nine were against copies of the agent itself, and the remaining five sets were against BIAI opponents.

We then collected an additional 36 trajectories, which were grouped into twelve sets of three using the same criteria. No trajectories were discarded from this second collection, all of which were races against BIAI opponents.

Of the final 79 trajectories, the agent’s car was drawn from a fixed set of 19 cars (as noted earlier). Across the two data collections, only two car types overlapped, resulting in eight trajectories for each of those car types. For the remaining car types, there were five trajectories per car type in the nine sets of five, except for the groupings that included discarded

trajectories, which contained four. In the twelve sets of three, each car type had three trajectories.

This grouping facilitated easier labeling by domain experts, who ranked trajectories within each group from most aggressive to most timid. These rankings were subsequently converted into pairwise preferences.



Figure 14: An illustration of the versus setup. The agent’s car (in red) is placed in last place to chase 19 opponents (in white cars) in a three-lap race. Each opponent is evenly spaced ahead of the agent. Copyright © 2025 Sony Interactive Entertainment Inc. Developed by Polyphony Digital Inc.

For the fast driving time-trial experiments, we leveraged the available BIAI agents to generate 56 time-trial trajectories using the same set of 19 cars. We then followed a similar protocol, randomly sampling groups of five trajectories and automatically ranking them by lap time, from fastest to slowest. Because groups were sampled with replacement, the same trajectories could appear in multiple groups, resulting in repeated pairwise orderings. To avoid over-representing redundant information, we retained each unique pairwise preference only once in the final dataset, resulting in the 1429 trajectories.

Table 5: Hyperparameters used for Soft-TAC and Cross-Entropy in Lunar Lander and GT experiments.

Method	Learning Rate	Batch Size
Lunar Lander		
SOFT-TAC	0.05	16
CROSS-ENTROPY	0.05	8
GT Fast Driving		
SOFT-TAC	0.05	8
CROSS-ENTROPY	0.03	8
GT Aggressive		
SOFT-TAC	0.05	4
CROSS-ENTROPY	0.05	8
GT Timid		
SOFT-TAC	0.05	4
CROSS-ENTROPY	0.05	4

D Training and Evaluation Details

D.1 Reward Learning

For the reward learning experiments, we considered only linear reward models and therefore did not use a neural network. We initialized the weights by sampling from a standard normal distribution $\mathcal{N}(0, 1)$ and applied weight clipping to keep the weights bounded in $[-200, 200]$ for Lunar Lander and $[0, 15]$ for GT. We trained the reward models using mini-batch gradient descent with the Adam optimizer [Kingma and Ba, 2015]. We tuned two hyperparameters—the learning rate and batch size—using a grid search. Specifically, we swept over learning rates in the set $\{0.01, 0.03, 0.05, 0.0001, 0.0003, 0.0005\}$. For batch size, we used different ranges depending on the experiment: for Lunar Lander, which had more trajectories in its preference dataset, we used $\{8, 16, 24\}$; In GT, for the aggressive-timid reward learning experiments we used $\{4, 8, 12\}$, and for the fast driving experiments, which had the largest preference dataset, we expanded the batch sizes to $\{8, 16, 32\}$. See Table 5 for the chosen hyperparameters.

For the temperature hyperparameter (α) used in both the Soft-TAC and Cross-Entropy loss functions, which scales differences in predicted returns, we fixed $\alpha = 1.0$. Since Cross-Entropy typically assumes $\alpha = 1.0$, we use the same value for Soft-TAC for consistency. For GT7 and Lunar Lander experiments, each model was trained for a maximum of 500 and 5000 epochs, respectively. However, to prevent overfitting, we employed early stopping during training. The early stopping procedure tracks the best model based on three metrics: TAC, accuracy, and loss. After each epoch, the model is considered to have improved if either of the following conditions holds:

1. TAC increases (or remains the same) *and* accuracy increases, or
2. TAC increases (or remains the same) *and* the loss decreases by more than a threshold of 0.0001.

Whenever an improvement is detected, the stored best model (including its metrics and weights) is updated and the counter of consecutive non-improving epochs is reset. If no improvement occurs, this counter is incremented. Training terminates once the model has failed to improve for 50 consecutive epochs, at which point early stopping is triggered and the best model observed during training is returned.

D.2 Learned Reward Functions

In Table 6, we present the learned weights for all eight reward features across all five seeds for both Soft-TAC and Cross-Entropy. For reference, we also include the default environment reward weights. Tables 8 and 7 report the corresponding learned reward parts for the GT experiments for all three seeds, covering both the aggressive-timid and the fast driving setting.

D.3 RL Training and Evaluation

For all experiments, we used a type of SAC algorithm and performed training asynchronously using a centralized

learner with distributed rollout workers. In the Lunar Lander experiments, training was run for 10,000 epochs, each consisting of 200 gradient steps. The learner used a single GPU with 8 GB of memory. Experience was collected by two rollout workers, each allocated one CPU with 2,048 MiB of memory. In the GT7 experiments, training was run for approximately 2,200 training epochs, each consisting of 6,000 gradient steps. Rollouts are conducted on 15 PlayStation consoles (PS4 and PS5—the only platforms that support the game). The learner used a single GPU and seven CPUs, with a total of 65 GB of memory allocated. Further details on the GT7 training setup can be found in Wurman *et al.* [2022]. See the hyperparameters used in Table 9.

D.4 Policy Selection

After training the RL policies, we then selected policies for evaluation based on certain criteria. In the Lunar Lander experiments, we did not employ a sophisticated policy selection procedure for evaluation. Instead, we evaluated five policies obtained near the end of training, corresponding to episodes 8,000, 8,500, 9,000, 9,500, and 10,000. This environment did not require specialized policy selection protocols, as the policies at convergence were qualitatively similar.

In contrast, prior work on GT7 has shown that even after training has converged, policies from different training checkpoints can exhibit subtle but meaningful differences in driving behavior [Wurman *et al.*, 2022]. Consequently, we used a similar policy selection protocol as Wurman *et al.* [2022]. More specifically, during training, we partially evaluated and saved the current policy (i.e., with exploration disabled) every five epochs. By partial evaluation, we mean that policies were evaluated on a small subset of cars rather than the full set of 552, as evaluating all cars at this frequency would be prohibitively expensive.

To select policies for evaluation, we employed a two-step selection protocol. First, we filtered candidate policies based on whether their evaluation metrics exceeded predefined thresholds, considering only metrics associated with the driving style of interest. For example, as time-trial tasks focused on fast driving, we required the BIAI ratio to be lower than 0.979. In versus tasks targeting aggressiveness or timidity, we considered metrics for overtaking attempts, lap time, and final place (as described in Appendix C.1). For aggressive behaviors, we filtered out the slowest 25% of policies based on final place and minimum lap time, as well as any policies with fewer than 7 overtaking attempts. For timid behaviors, we selected policies that had the lowest 15% of overtaking attempts. We found that using these distinct criteria produced the most aggressive and most timid policies, rather than simply taking opposite extremes of the same metrics.

Second, among the filtered policies, we performed a full evaluation on all 552 cars and selected the best policy to report. By best, we mean the policy that achieved the most favorable metrics for the task. For the time-trial task, we selected the policy with the fastest lap time; for the aggressive-timid experiments, we selected policies exhibiting the most aggressive or timid behaviors. Figure 15 shows examples of aggressive and timid driving learned with the Soft-TAC objective.

Table 6: Learned Lunar Lander reward weights (Soft-TAC, Cross-Entropy, and Default) and resulting TAC scores.

Distance	Speed	Tilt	Leg Contact	Side Engine	Main Engine	Crash	Safe Landing	TAC
SOFT-TAC								
-11.22	-3.52	-3.18	-0.63	0.02	-0.26	-26.82	43.06	0.84
-4.26	-1.56	-3.26	1.72	-0.05	-0.06	-9.77	8.79	0.84
-3.60	-0.39	-5.69	1.70	0.04	-0.08	-11.56	11.29	0.82
-3.64	-1.92	-3.36	0.93	-0.05	-0.06	-8.09	8.09	0.82
-5.56	0.20	-2.31	0.34	0.05	-0.11	-12.19	12.43	0.81
CROSS-ENTROPY								
-5.12	-1.24	-0.65	2.18	-0.05	-0.08	-14.16	29.49	0.85
-2.56	-1.61	-4.05	1.70	-0.00	-0.15	-13.62	32.03	0.84
-1.84	-0.64	-1.70	1.00	-0.01	-0.02	-3.94	4.25	0.82
-4.06	-2.02	-2.73	3.11	-0.08	-0.07	-11.82	12.88	0.82
-3.57	-0.03	-2.31	0.79	-0.00	-0.04	-6.19	7.38	0.80
DEFAULT								
-100.0	-100.0	-100.0	10.0	-0.03	-0.3	-100.0	100.0	0.62

Table 7: GT7 controlling aggressiveness and timidness: learned reward weights and resulting TAC scores.

Experiment	Method	Overtaking	Collision	TAC
AGGRESSIVE	SOFT-TAC	0.05	2.73	0.77
		0.09	2.80	0.77
		0.03	2.75	0.77
	CROSS-ENTROPY	0.0	1.73	0.67
		0.0	1.36	0.69
		0.0	1.18	0.56
TIMID	SOFT-TAC	2.47	0.0	-0.27
		2.49	0.0	-0.27
		2.20	0.0	-0.27
	CROSS-ENTROPY	0.82	0.0	-0.32
		0.82	0.0	-0.32
		0.83	0.0	-0.32



(a)



(b)

Figure 15: Example Soft-TAC learned driving style for aggressive (a) and timid (b). An aggressive agent will engage with opponents and attempt to overtake, resulting in more car interactions such as collisions. Whereas a timid agent will keep a distance from opponents, with minimal car contacts.

E Additional Results

E.1 Generalization of Learned Reward Models

In GT7, we were also interested in whether reward functions learned from preferences on a single track can gener-

Table 8: GT7 fast driving experiments: learned progress weights and resulting TAC scores.

Method	Progress	TAC
SOFT-TAC	7.98	0.97
	7.23	0.97
	7.62	0.97
CROSS-ENTROPY	0.47	0.965
	0.50	0.965
	0.51	0.965

alize to produce effective policies on an unseen track—that is, whether the learned reward functions are specific to the track in the preference dataset. We tested this in the fast driving time-trial experiment. In this experiment, we reused the reward function that was learned only using the preference dataset collected on the Sarthe track to train a QR-SAC agent on the Autodrome Lago Maggiore (Maggiore) track. We chose Maggiore because of its technical layout, including complex cornering sequences and elevation management. These track characteristics contrast with the high-speed, longitudinal nature of Sarthe. This setup allows us to assess whether reward functions can generalize to tracks that differ from those used during preference collection. The three metrics (BIAI ratio, lap time, and number of incomplete laps) reported in Table 10 show that the reward model trained on Sarthe track preferences can still produce effective policies on the Maggiore track. In particular, reward models trained with Soft-TAC reduced the average lap time by 1.4 seconds compared to Cross-Entropy and outperformed the default reward by 0.4 seconds. Reported metrics exclude incomplete laps that exceed the 1800-second threshold; this never occurred with Soft-TAC, but did with the other baselines.

E.2 Empirical Robustness of TAC

We performed two ablations to further evaluate the robustness of TAC. First, we examined how TAC is affected by the number of human preferences used in its computation. Using the human preference dataset from the aggressive–timid reward learning experiment, we randomly sampled 30 sets of preferences with sample sizes of 25, 50, 75, and 100 from the full set of 118. Separately, we randomly sampled reward weights for the overtaking and collision features to generate multiple reward functions (each shown in an individual plot in Figure 16). TAC scores were then computed for each reward function using the different preference sample sizes. We found that the average TAC score remained largely consistent across all tested sample sizes, while the standard error decreased as the number of preferences increased. This result indicates that TAC is robust even when the preference dataset was small, making it suitable for domains where collecting preference data is challenging.

For the second ablation, we examined the effect of trajectory length on TAC by reusing the same aggressive–timid preferences collected over full trajectories, while varying only the length of the trajectory segments used to compute TAC. In our main experiments (Sections 5.2 and 5.3), pref-

erences were elicited over entire trajectories, whereas prior PbRL work often considers preferences over shorter trajectory segments. Accordingly, in this ablation, we fix the preference dataset and vary only the trajectory length. GT7 trajectories are relatively long, ranging from 2,040 to 12,407 time steps; here, we computed TAC scores using trajectory segments of length 50, 100, 150, 250, 300, 500, and 1,000 time steps, extracted from the original trajectories. As shown in Figure 17, TAC was also robust to the trajectory length: using segment lengths of at least 500 time steps produced results comparable to full trajectories, which are much shorter segments compared to full GT7 trajectories. Segments shorter than 500 yielded lower similarity, which is expected because the human preferences were expressed over entire trajectories, and shorter segments may not capture sufficient behavioral information to reflect those preferences.

Table 9: RL Hyperparameters used in both GT7 and Lunar Lander experiments.

Hyperparameter	GT7	Lunar Lander
RL Algorithm	QR-SAC [Wurman <i>et al.</i> , 2022]	SAC [Haarnoja <i>et al.</i> , 2018]
Optimizer	Adam [Kingma and Ba, 2015]	Adam
Number of Quantiles	32	NA
Number of Critic Networks	2	2
Number of Target Critic Networks	2	2
Number of Policy Networks	1	1
Learnable Entropy	False	True
Fixed Entropy Regularization Coefficient	0.01	N/A
Entropy Learning Rate	N/A	1×10^{-4}
Target Entropy	N/A	-2
Critic Learning Rate	2.5×10^{-5}	5×10^{-4}
Actor Learning Rate	1.25×10^{-5}	5×10^{-4}
Target Critics Update Rate	0.005	0.005
Discount Factor	0.9896	0.99
Batch Size	512	32
Replay Buffer Size	10000000	20000
Global Norm of Critics Gradient Clipping	10.0	10.0
Number of Training Epochs	~2200	10000
Number of Gradient Steps per Epoch	6000	200

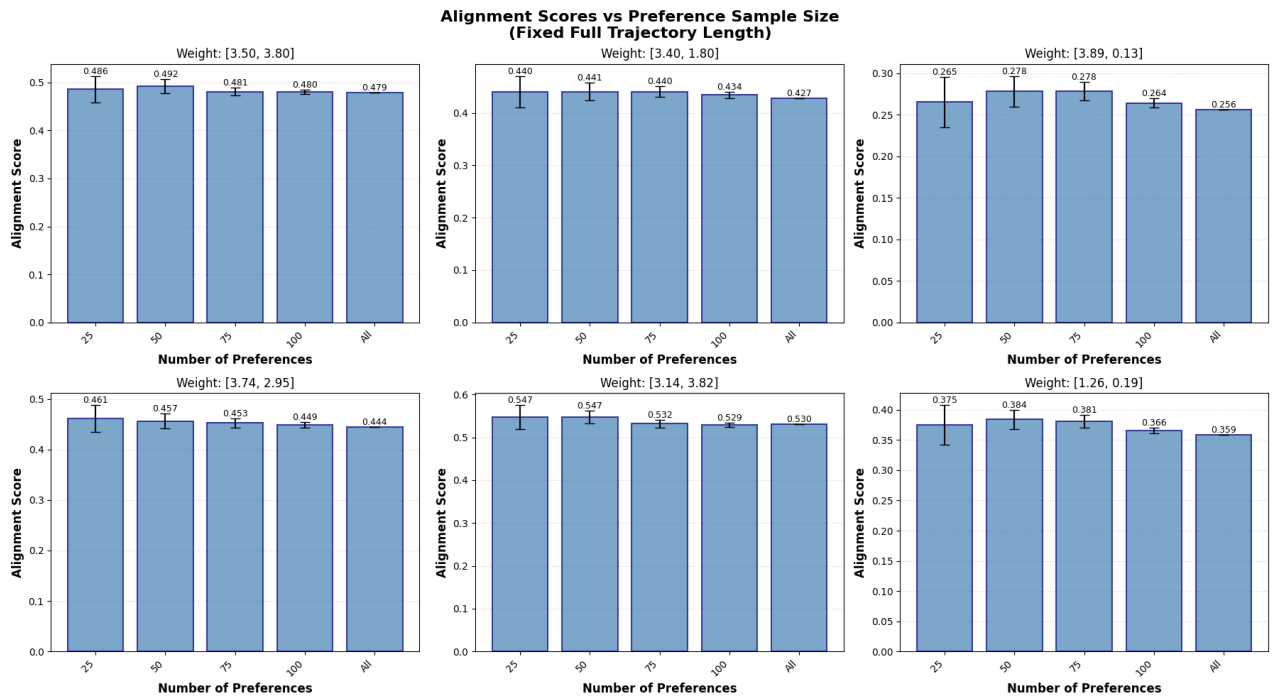


Figure 16: Average TAC (\pm SE) versus Number of Human Preferences in GT7

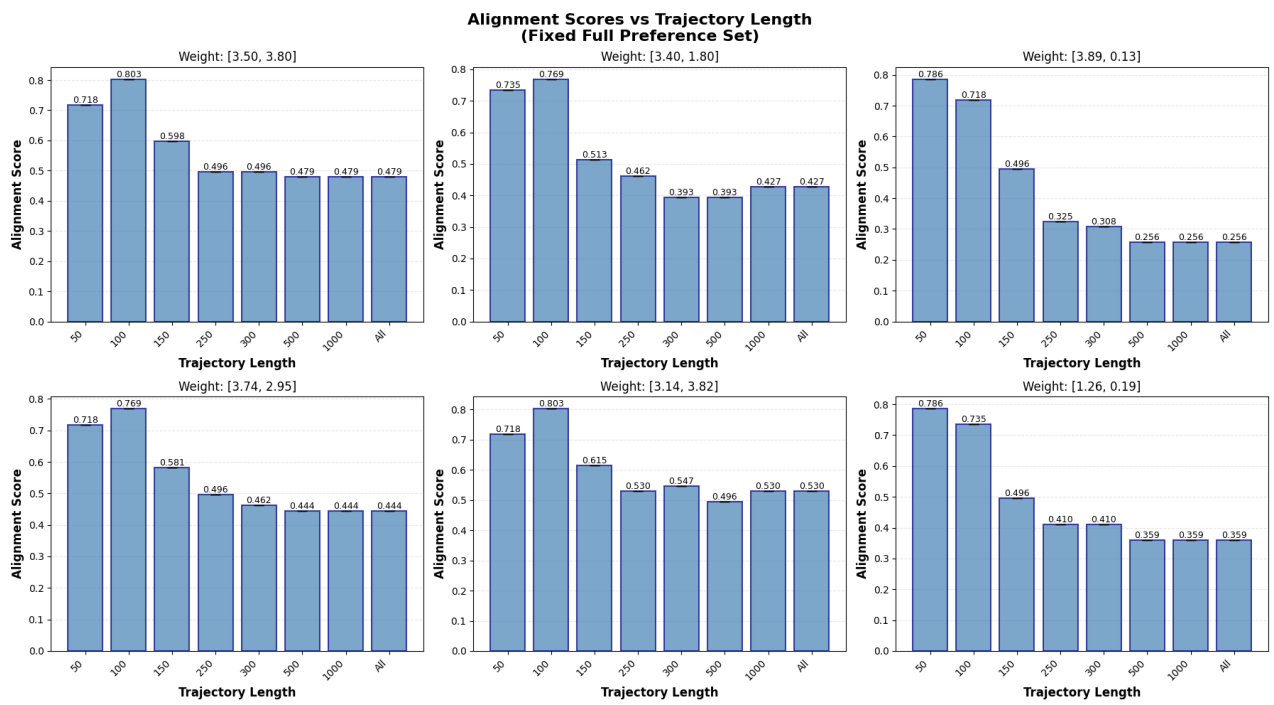


Figure 17: TAC versus Trajectory Length in GT7

Table 10: BIAI ratio (\pm SE), minimal lap time (\pm SE), and number of incomplete laps after RL training with each reward (lower is better) on the Maggiore track for the time-trial task in GT7.

Method	BIAI Ratio	Lap Time	Lap Time > 1800
SOFT-TAC	0.980 ± 0.00	135.85 ± 0.20	0
CROSS-ENTROPY	0.990 ± 0.00	137.39 ± 0.31	15
DEFAULT	0.983 ± 0.00	136.33 ± 0.11	1